Analysis of the configurational temperature of polymeric liquids under shear and elongational flows using nonequilibrium molecular dynamics and Monte Carlo simulations

Chunggi Baig[1,a] and Brian J. Edwards[2,b]
[1]*Department of Chemical Engineering, University of Patras and FORTH-ICE/HT, Patras GR 26504, Greece*
[2]*Department of Chemical and Biomolecular Engineering, University of Tennessee, Knoxville, Tennessee 37996, USA*

(Received 11 November 2009; accepted 2 April 2010; published online 14 May 2010)

We present a detailed analysis of the configurational temperature (T_{conf}) for its application to polymeric materials using nonequilibrium molecular dynamics (NEMD) and nonequilibrium Monte Carlo (NEMC) methods. Simulations were performed of linear polyethylene liquid $C_{78}H_{158}$ undergoing shear and elongational flows. At equilibrium, T_{conf} is equal to the set point temperature of the simulation. An aphysically large decrease in T_{conf} is observed in the NEMD simulations for both flows, especially at strong flow fields. By analyzing separately the individual contributions of the different potential interaction modes to the configurational temperature, it is found that the bonded modes (which constitutes almost 99.5% of the total) dominate the total T_{conf} over the nonbonded ones; i.e., bond-stretching ($\approx$86.5%), bond-bending ($\approx$11.8%), bond-torsional ($\approx$1.2%), nonbonded intermolecular ($\approx$0.4%), and intramolecular ($\approx$0.1%) Lennard-Jones. The configurational temperature of the individual modes generally exhibits a nonmonotonic behavior with the flow strength and a dramatic change beyond a critical value of flow strength; this is mainly attributed to the dynamical effect of strong molecular collisions occurring at strong flow fields. In contrast, no such behavior is observed in the NEMC simulations where such dynamical effects are absent. Based on the principal physical concept of the configurational temperature, which represents the large-scale structural characteristics of the system, we propose to exclude the dynamical effects exhibited by the individual interaction modes, in obtaining a physically meaningful T_{conf} as the configurational entropy of the system should not be affected by such factors. Since (a) the main difference between equilibrium and nonequilibrium states lies in the change in the overall (global) structure (represented by the bond torsional and nonbonded modes), and (b) the local, very short structure (represented by the bond-stretching and bond-bending modes) is barely changing between equilibrium and nonequilibrium states and its contribution to the total system configurational entropy is negligible compared to the large-scale structural changes, in order to accurately describe the structural changes occurring at nonequilibrium states by use of the configurational temperature, we further propose that only the contributions from the bond-torsional and nonbonded modes to ΔT_{conf} between equilibrium and nonequilibrium states should be taken into account to generate a physically meaningful ΔT_{conf}. Applying the above hypothesis to the analysis of the simulation data, good agreement between the NEMD and NEMC simulations (and between NEMD simulations for different flows) is observed. Furthermore, the configurational temperature obtained in such way is found to match remarkably well with the heat capacity of amorphous polyethylene liquids and the flow-enhanced melting-point elevation reported in experiment. © *2010 American Institute of Physics*. [doi:10.1063/1.3415085]

I. INTRODUCTION

Traditionally the temperature is considered as a thermodynamic quantity representing the average kinetic energy per degree of freedom of the system. At the same time, it is also well recognized as a physical quantity associated with the potential energy of the system via the well-known classical virial theorem[1] or the generalized equipartition theorem.[2] This dual nature of the temperature has been nicely reconciled by Rugh,[3] who demonstrated that the temperature can be calculated from a geometric structure of the energy surface of the system using the thermodynamic relation of temperature $(1/T=\partial S/\partial E)$ and the fundamental expression of entropy $S_E=k_B \ln[\int \delta(H(\mathbf{\Gamma})-E)d\mathbf{\Gamma}]+C$ for an isolated system with the Hamiltonian H, being equal to the energy E, and k_B is the Boltzmann constant. In this expression, C is a constant and $\mathbf{\Gamma}$ denotes the phase space consisting of all the

[a]Author to whom correspondence should be addressed. Electronic mail: cbaig@iceht.forth.gr. Tel.: +30-2610-965219. FAX: +30-2610-965223.
[b]Electronic mail: bje@utk.edu. Tel.: +1-865-974-9596. FAX: +1-865-974-7076.

positions $\{\mathbf{r}\}$ and momenta $\{\mathbf{p}\}$ of the particles in the system. Rugh derived a fundamental equation for the temperature of a material,

$$\frac{1}{k_B T} = \left\langle \nabla \cdot \left(\frac{\nabla H}{|\nabla H|^2} \right) \right\rangle, \tag{1}$$

where the angular brackets represent an ensemble average, and the gradient vector involves all the degrees of freedom in $\mathbf{\Gamma}$. It is thus seen that the intrinsic structure of the energy surface of the system is directly related to the system's temperature.

Evans and co-workers[4,5] recognized the importance of the above expression and demonstrated its great potential value in practical applications using Monte Carlo[4] (MC) and molecular dynamics[5] (MD) simulations of simple fluids. A further generalization of Rugh's discovery was carried out by Jepps *et al.*,[6] who derived the equation

$$\frac{1}{k_B T} = \frac{\langle \nabla \cdot \mathbf{B}(\mathbf{\Gamma}) \rangle}{\langle \nabla H \cdot \mathbf{B}(\mathbf{\Gamma}) \rangle}, \tag{2}$$

where $\mathbf{B}(\mathbf{\Gamma})$ is an arbitrary vector field with the restrictions such that both the numerator and the denominator be larger than zero and finite, and that the numerator grows more slowly than e^N, with N being the number of atoms in the system. They showed that Eq. (2) is valid not only for the microcanonical ensemble but also for other statistical ensembles (e.g., canonical, grand canonical, etc.). They further showed that with a proper choice of $\mathbf{B}(\mathbf{\Gamma})$ accounting for the periodicity, it can also be applied to a periodic system employed in practical MD and MC simulations. It is also recognized that with the special choice of $\mathbf{B}(\mathbf{\Gamma}) = \nabla H / |\nabla H|^2$, Eq. (2) is the same as the original expression, Eq. (1).

A particularly important expression regarding the temperature arises with the choice of $\mathbf{B}(\mathbf{\Gamma}) = \nabla U$, where $U = U(\mathbf{r}_1, \mathbf{r}_2, \ldots, \mathbf{r}_N)$ is the potential energy of an N-particle system,

$$\frac{1}{k_B T_{\text{conf}}} = -\frac{\left\langle \sum_{i=1}^{N} \nabla_i \cdot \mathbf{F}_i \right\rangle}{\left\langle \sum_{i=1}^{N} \mathbf{F}_i^2 \right\rangle}. \tag{3}$$

In this expression, $\mathbf{F}_i$ is the total interaction force acting on particle i. In this equation, T_{conf} is called the "configurational temperature" since it is only related to the system configuration based on the particle positions without regard to the particle momenta. The configurational temperature calculated by Eq. (3) is known to be very accurate [i.e., close to the temperature calculated from Eq. (1) and also the kinetic temperature] and statistically reliable (i.e., less affected by system-size effects), and thus has been applied to various physical systems (e.g., chain molecules,[7] confined fluids,[8] charge-stabilized colloidal systems,[9] polypeptides,[10] gravitationally driven inhomogeneous systems,[11] etc.) under equilibrium or nonequilibrium conditions. Recently, the configurational temperature expression has been further extended for physical systems involving hard-core or discontinuous potentials.[12] Also, Braga and Travis[13] derived a set of evolution equations incorporating the Nosé–Hoover thermostat algorithm based on the configurational temperature. Accordingly, Eq. (3) is adopted in this study for the analysis of the configurational temperature.

The configurational temperature has also been applied to nonequilibrium systems under flow.[5,7,8,14] In particular, Delhommelle and Evans[14] carried out direct nonequilibrium MD (NEMD) simulations of a short n-alkane (decane) under shear flow and investigated the relationship between the configurational temperature (T_{conf}) and the kinetic temperature (T_{kin}, which is based on the center-of-mass molecular kinetic energy) with respect to the flow field. They observed that while T_{conf} is close to the imposed T_{kin} at low shear rates, it deviates (increases) significantly from the set value of T_{kin} at high shear rates (with increasing the shear rate), and vice versa. They ascribed this phenomenon to the insufficiency of the molecular kinetic thermostat for removing the heat from all the internal (atomistic) degrees of freedom under strong flow fields. Although their interpretation is considered to be correct (as they further analyzed it in later work[15]), a further analysis is necessary for a deeper understanding of the microscopic origins. We address this issue here through a detailed analysis of the results from NEMD (Ref. 16) and nonequilibrium MC (NEMC) (Ref. 17) simulations of a short, unentangled ($C_{78}H_{158}$) linear polyethylene liquid under shear, as well as under planar and uniaxial elongational flows; i.e., the individual contributions of different interaction modes to the configurational temperature are separately analyzed using the analytical formulas derived in Sec. II.

In conjunction with the use of the temperature expressions [Eqs. (1)–(3)] for nonequilibrium systems under external flow fields in this study, we note some subtle points. As has been well recognized by researchers in the nonequilibrium thermodynamics and statistical mechanics in the past, there still remains a certain degree of ambiguity in the definition and the operative concept of the system temperature of nonequilibrium states. Whereas all the different definitions for the temperature (e.g., $1/T = \partial S/\partial E$, Lagrange multiplier to the system energy, the average kinetic energy per degree of freedom or equipartition theorem, and the thermodynamic force for the heat flux) have rigorously proven to be the same as each other under equilibrium conditions, they are generally considered to be different in nonequilibrium states. These quantitative differences depend on the applied field strength and may be dependent on the applied thermodynamic formalism; for example, using extended irreversible thermodynamics,[18] Casas-Vázquez and Jou[19] showed that the temperature based on the heat flux or $1/T = \partial S/\partial E$ with the nonequilibrium entropy is calculated as smaller (at least by the second order of perturbations or heat fluxes) than the temperature based on the kinetic energy. On the basis of advanced nonequilibrium thermodynamic frameworks beyond linear irreversible thermodynamics[20] (such as the extended irreversible thermodynamics,[18] the matrix model,[21] the generalized bracket formalism,[22] and the GENERIC formalisms[23]), an implicit assumption in applying Eqs. (1)–(3) to nonequilibrium systems is essentially that the dependence of the nonequilibrium entropy on the external perturbations is not affected by the energy content of the system.

Furthermore, by invoking the assumption of a local or quasithermodynamic equilibrium but with an extended form

of fundamental thermodynamic relations [e.g., Eqs. (14a)–(14c), (15a), (15b), (16a), and (16b) below], the original idea of the configurational temperature developed under the equilibrium conditions can be extended to flowing nonequilibrium systems, which is standard protocol in modern nonequilibrium thermodynamic formalisms.[18,21–23] Accordingly, by expanding the statistical ensemble [see, for example, Eq. (17) below], we can reformulate the expressions of the configurational temperature for nonequilibrium systems under an external field. In Appendix A, we derive a generalized expression for the configurational temperature by employing a generalized statistical canonical ensemble accounting for all the (extensive) thermodynamic state variables and the associated thermodynamic fields (Lagrange multipliers).

This paper is organized as follows. In Sec. II, we present the analytical expressions of calculating T_{conf} for each individual interaction mode. (The detailed derivations are provided in Appendix B.) In Sec. III, we describe the simulation (NEMD and NEMC) methodology and the systems employed in this study. The simulation results are presented in Sec. IV, and a summary is offered in Sec. V.

II. ANALYTICAL FORMULAS FOR THE CONFIGURATIONAL TEMPERATURE MODES

In this section, we present the analytical expressions that enable us to investigate separately the individual contributions to the configurational temperature from the individual interaction modes that are typically involved in the simulation of polymeric materials [i.e., the bond-stretching, bond-bending, bond-torsional, and nonbonded Lennard-Jones (LJ) interactions].[24] The configurational temperature of each mode can then be expressed formally as

$$\frac{1}{k_B T_{\text{conf,type}}} = -\frac{\langle \sum_{i=1}^{N} \nabla_i \cdot \mathbf{F}_{i,\text{type}} \rangle}{\langle \sum_{i=1}^{N} \mathbf{F}_{i,\text{type}}^2 \rangle}. \tag{4}$$

Since the analytical expressions for the force shown in the denominator on the right side of Eq. (4) can be readily derived, here we focus only on the formula for $\nabla \cdot \mathbf{F}$. (We should note that the total T_{conf} would not be a simple combination of the individual types, as a coupling between different interaction modes occurs.)

In the derivation of the analytical formula for $\nabla \cdot \mathbf{F}$, it is convenient to use the relative position vectors and the center-of-mass position vector ($\mathbf{R}_G$) of the particles since the potentials used herein (and therefore the forces as well) are typically independent of $\mathbf{R}_G$ (i.e., homogeneity of space). For the bond-bending interaction, for example, the convenient set of variables would be $\{\mathbf{r}_1-\mathbf{r}_2, \mathbf{r}_2-\mathbf{r}_3, \mathbf{R}_G\}$ instead of $\{\mathbf{r}_1, \mathbf{r}_2, \mathbf{r}_3\}$. All the potentials and forces considered here are assumed to be independent of $\mathbf{R}_G$.

Let us first consider the simplest case of the two-body interaction modes, such as the bond-stretching and the nonbonded LJ interactions, which are further assumed to be dependent only on the magnitude (r_{12}) of the relative position vector ($\mathbf{r}_{12} \equiv \mathbf{r}_1-\mathbf{r}_2$) but not the direction. Together with Newton's third law (i.e., $\mathbf{F}_2=-\mathbf{F}_1$), we can derive the following expression for $\nabla \cdot \mathbf{F}$. (The detailed derivation is presented in Appendix B.)

$$\nabla \cdot \mathbf{F} = -2\left(\frac{d^2U(r_{12})}{dr_{12}^2} + \frac{2}{r_{12}} \frac{dU(r_{12})}{dr_{12}} \right). \tag{5}$$

As an example, for a harmonic bond-stretching potential $U_{\text{str}}(r_{12})=k_{\text{str}}(r_{12}-r_{\text{eq}})^2/2$, Eq. (5) gives rise to

$$\nabla \cdot \mathbf{F} = -2k_{\text{str}}\left(1 + \frac{2}{r_{12}}(r_{12}-r_{\text{eq}}) \right). \tag{6}$$

Similarly, we derive the expression of $\nabla \cdot \mathbf{F}$ for the nonbonded LJ interaction.

For the bond-bending interaction where three atoms are involved, we use $\{\mathbf{a}, \mathbf{b}, \mathbf{R}_G\}$ for the basis set of variables where $\mathbf{a}=\mathbf{r}_1-\mathbf{r}_2$, $\mathbf{b}=\mathbf{r}_3-\mathbf{r}_2$, and $\mathbf{R}_G=(\mathbf{r}_1+\mathbf{r}_2+\mathbf{r}_3)/3$ rather than the original set $\{\mathbf{r}_1, \mathbf{r}_2, \mathbf{r}_3\}$. Through the transformation rule between the two sets [see Eqs. (B4)–(B6)], $\nabla \cdot \mathbf{F}$ is found to be

$$\begin{aligned}
\nabla \cdot \mathbf{F} &= \frac{\partial}{\partial \mathbf{r}_1} \cdot \mathbf{F}_1 + \frac{\partial}{\partial \mathbf{r}_2} \cdot \mathbf{F}_2 + \frac{\partial}{\partial \mathbf{r}_3} \cdot \mathbf{F}_3 \\
&= -2\left(\frac{\partial}{\partial \mathbf{a}} \cdot \frac{\partial U_{\text{ben}}}{\partial \mathbf{a}} + \frac{\partial}{\partial \mathbf{a}} \cdot \frac{\partial U_{\text{ben}}}{\partial \mathbf{b}} + \frac{\partial}{\partial \mathbf{b}} \cdot \frac{\partial U_{\text{ben}}}{\partial \mathbf{b}} \right) \\
&= -2\left\{ \frac{\partial}{\partial \cos\theta}\left(\frac{\partial U_{\text{ben}}}{\partial \cos\theta} \right) \left[\left(\frac{\partial \cos\theta}{\partial a_\alpha} \right)\left(\frac{\partial \cos\theta}{\partial a_\alpha} \right) \right.\right. \\
&\quad \left. + \left(\frac{\partial \cos\theta}{\partial a_\alpha} \right)\left(\frac{\partial \cos\theta}{\partial b_\alpha} \right) + \left(\frac{\partial \cos\theta}{\partial b_\alpha} \right)\left(\frac{\partial \cos\theta}{\partial b_\alpha} \right) \right] \\
&\quad \times \left(\frac{\partial U_{\text{ben}}}{\partial \cos\theta} \right) \left[\frac{\partial}{\partial a_\alpha}\left(\frac{\partial \cos\theta}{\partial a_\alpha} \right) + \frac{\partial}{\partial a_\alpha}\left(\frac{\partial \cos\theta}{\partial b_\alpha} \right) \right. \\
&\quad \left.\left. + \frac{\partial}{\partial b_\alpha}\left(\frac{\partial \cos\theta}{\partial b_\alpha} \right) \right] \right\},
\end{aligned} \tag{7}$$

where $\cos\theta=\mathbf{a}\cdot\mathbf{b}/(|\mathbf{a}||\mathbf{b}|)$. Using Eqs. (B10)–(B12) in Appendix B for the first and the second derivatives of $\cos\theta$ with respect to $\mathbf{a}$ and $\mathbf{b}$, we obtain the expression for $\nabla \cdot \mathbf{F}$ as

$$\begin{aligned}
\nabla \cdot \mathbf{F} = -2\left\{ \left(\frac{\partial^2 U_{\text{ben}}}{\partial \theta^2} \right)\left(\frac{1}{|\mathbf{a}|^2} + \frac{1}{|\mathbf{b}|^2} - \frac{\cos\theta}{|\mathbf{a}||\mathbf{b}|} \right) \right. \\
\left. + \frac{\cos\theta}{\sin\theta} \frac{\partial U_{\text{ben}}}{\partial \theta}\left(\frac{1}{|\mathbf{a}|^2} + \frac{1}{|\mathbf{b}|^2} - \frac{1}{|\mathbf{a}||\mathbf{b}|\cos\theta} \right) \right\}.
\end{aligned} \tag{8}$$

Equation (8) can be applied to an arbitrary form of the bending potential as a function of θ; e.g., for a simple harmonic bending potential such as $U_{\text{ben}}(\theta)=k_{\text{ben}}(\theta-\theta_{\text{eq}})^2/2$, it becomes

$$\begin{aligned}
\nabla \cdot \mathbf{F} = -2k_{\text{ben}}\left\{ \left(\frac{1}{|\mathbf{a}|^2} + \frac{1}{|\mathbf{b}|^2} - \frac{\cos\theta}{|\mathbf{a}||\mathbf{b}|} \right) \right. \\
\left. + \frac{\cos\theta}{\sin\theta}\left(\frac{1}{|\mathbf{a}|^2} + \frac{1}{|\mathbf{b}|^2} - \frac{1}{|\mathbf{a}||\mathbf{b}|\cos\theta} \right)(\theta-\theta_{\text{eq}}) \right\}.
\end{aligned} \tag{9}$$

Lastly, for the bond-torsional interaction where four atoms are involved, the variable set is chosen as $\{\mathbf{a},\mathbf{b},\mathbf{c},\mathbf{R}_G\}$, where $\mathbf{a}=\mathbf{r}_1-\mathbf{r}_2$, $\mathbf{b}=\mathbf{r}_2-\mathbf{r}_3$, $\mathbf{c}=\mathbf{r}_3-\mathbf{r}_4$, and $\mathbf{R}_G=(\mathbf{r}_1+\mathbf{r}_2+\mathbf{r}_3+\mathbf{r}_4)/4$. A similar procedure as in the bond-bending mode case leads to the following expression for $\nabla\cdot\mathbf{F}$ (refer to Appendix B for details):

$$\nabla\cdot\mathbf{F}=\frac{\partial}{\partial\mathbf{r}_1}\cdot\mathbf{F}_1+\frac{\partial}{\partial\mathbf{r}_2}\cdot\mathbf{F}_2+\frac{\partial}{\partial\mathbf{r}_3}\cdot\mathbf{F}_3+\frac{\partial}{\partial\mathbf{r}_4}\cdot\mathbf{F}_4=-2\frac{\partial}{\partial\cos\phi}\left(\frac{\partial U_{\mathrm{tor}}}{\partial\cos\phi}\right)\left[\left(\frac{\partial\cos\phi}{\partial a_\alpha}\right)\left(\frac{\partial\cos\phi}{\partial a_\alpha}\right)+\left(\frac{\partial\cos\phi}{\partial b_\alpha}\right)\left(\frac{\partial\cos\phi}{\partial b_\alpha}\right)+\left(\frac{\partial\cos\phi}{\partial c_\alpha}\right)\left(\frac{\partial\cos\phi}{\partial c_\alpha}\right)-\left(\frac{\partial\cos\phi}{\partial a_\alpha}\right)\left(\frac{\partial\cos\phi}{\partial b_\alpha}\right)-\left(\frac{\partial\cos\phi}{\partial b_\alpha}\right)\left(\frac{\partial\cos\phi}{\partial c_\alpha}\right)\right]-2\left(\frac{\partial U_{\mathrm{tor}}}{\partial\cos\phi}\right)\left[\frac{\partial}{\partial a_\alpha}\left(\frac{\partial\cos\phi}{\partial a_\alpha}\right)+\frac{\partial}{\partial b_\alpha}\left(\frac{\partial\cos\phi}{\partial b_\alpha}\right)+\frac{\partial}{\partial c_\alpha}\left(\frac{\partial\cos\phi}{\partial c_\alpha}\right)-\frac{\partial}{\partial a_\alpha}\left(\frac{\partial\cos\phi}{\partial b_\alpha}\right)-\frac{\partial}{\partial b_\alpha}\left(\frac{\partial\cos\phi}{\partial c_\alpha}\right)\right],\tag{10}$$

where $\cos\phi=(\mathbf{a}\times\mathbf{b})\cdot(\mathbf{b}\times\mathbf{c})/|\mathbf{a}\times\mathbf{b}||\mathbf{b}\times\mathbf{c}|$ (taking $\phi=0$ as the *cis*-configuration). In order to evaluate $\nabla\cdot\mathbf{F}$, we need to know the formula for the first and the second derivatives of $\cos\phi$ with respect to $\{\mathbf{a},\mathbf{b},\mathbf{c}\}$. To save space in the main text, we provide all the formulas in Appendix B [see Eqs. (B33)–(B45)], with which $\nabla\cdot\mathbf{F}$ can be calculated for an arbitrary form of $U_{\mathrm{tor}}(\phi)$.

III. SIMULATION METHODOLOGY AND SYSTEMS STUDIED

A. Simulation methodology

The following set of evolution equations (p-SLLOD algorithm[16] with the Nosé–Hoover thermostat[25]) was employed in NEMD simulations at constant temperature and density,[26]

$$\begin{aligned}\dot{\mathbf{q}}_{ia}&=\frac{\mathbf{p}_{ia}}{m_{ia}}+\mathbf{q}_{ia}\cdot\nabla\mathbf{u},\\ \dot{\mathbf{p}}_{ia}&=\mathbf{F}_{ia}-\mathbf{p}_{ia}\cdot\nabla\mathbf{u}-m_{ia}\mathbf{q}_{ia}\cdot\nabla\mathbf{u}\cdot\nabla\mathbf{u}-\frac{p_\zeta}{Q}\mathbf{p}_{ia},\\ \dot{\zeta}&=\frac{p_\zeta}{Q},\\ \dot{p}_\zeta&=\sum_i\sum_a\frac{\mathbf{p}_{ia}^2}{m_{ia}}-dnk_BT,\end{aligned}\tag{11}$$

where $\mathbf{q}_{ia}$, $\mathbf{p}_{ia}$, and $\mathbf{F}_{ia}$ are the position, momentum, and force vectors of atom a in molecule i, of mass m_{ia}. The d denotes the dimensionality, and n the total number of atoms. ζ and p_ζ are, respectively, coordinatelike and momentumlike variables of the Nosé–Hoover thermostat, which controls the temperature of system at a desired level. (It is known to be the only one that can generate the true canonical ensemble, i.e., constant T and ρ.[25]) $Q=dNk_BT\tau^2$ (τ, the relaxation time parameter) is the mass parameter of the thermostat. $\nabla\mathbf{u}$ represents the velocity gradient tensor of the imposed flow field:

$$\nabla\mathbf{u}=\begin{bmatrix}0&0&0\\ \dot{\gamma}&0&0\\ 0&0&0\end{bmatrix}\quad\text{for planar shear flow (PCF)},\tag{12a}$$

$$\nabla\mathbf{u}=\begin{bmatrix}\dot{\varepsilon}&0&0\\ 0&-\dot{\varepsilon}&0\\ 0&0&0\end{bmatrix}\quad\text{for planar elongational flow (PEF)}.\tag{12b}$$

Note that the term $m_{ia}\mathbf{q}_{ia}\cdot\nabla\mathbf{u}\cdot\nabla\mathbf{u}$ in the momentum equation in Eq. (11) vanishes for planar Couette flow (PCF).

The above equations of motion [Eq. (11)] were integrated by an efficient multiple time step algorithm, the r-RESPA (reversible reference system propagator algorithm),[27] where two different time scales for a MD step were used; the large one for the slowly varying forces (corresponding to the nonbonded intermolecular and intramolecular LJ interactions, Nosé–Hoover thermostat, and the flow field) and the small one for the rapidly varying forces (involving the bond-stretching, bond-bending, and bond-torsional interactions); the large and small time steps were, respectively, 2.39 and 0.48 fs for PCF, and 2.30 fs and 0.46 fs for planar elongational flow (PEF). The relaxation time parameter τ of the thermostat was set equal to 0.24 ps.

The boundary conditions used in the NEMD simulations were the well-known Lees–Edwards boundary conditions[28] for PCF and the Kraynik–Reinelt boundary conditions[29] (KRBCs) for PEF. In applying the KRBCs, we chose the following set of the three integer parameters in Ref. 29: $k=3$, $N_{11}=2$, and $N_{12}=-1$. This is known to be a good set in the case of the square lattice in the extensional plane (i.e., the x and y dimensions of the simulation box are the same) undergoing planar elongation, leading to the Hencky strain $\varepsilon_p\approx0.9624$ for the spatial periodicity and the initial orientation angle of the simulation box $\theta_0\approx31.718°$. The time period t_p for the temporal periodicity in the KRBCs was then determined from $\varepsilon_p=\dot{\varepsilon}t_p$. For details of the KRBCs, we refer readers to the original article.[29] Furthermore, for details of the implementation of the KRBCs in NEMD simulations, readers are referred to the literature.[16,26,30]

In addition to the NEMD simulations, NEMC simulations were performed using a recently developed thermodynamically well-founded MC (the so-called GENERIC MC) methodology,[17,31] the underlying principles of which are based on a rigorous formulation of nonequilibrium thermodynamics.[23] Since the detailed fundamental aspects of the GENERIC MC method can be found in the literature,[17,31] here we present only some basic equations that are directly involved in the simulations. As a nonequilibrium structural thermodynamic variable, we adopted the second-rank conformation tensor $\tilde{\mathbf{c}}$, which is defined as[22,32,33]

$$\tilde{c}_{\alpha\beta} = \frac{3\langle R_\alpha R_\beta \rangle}{\langle R^2 \rangle_{\mathrm{eq}}}, \tag{13}$$

where $\mathbf{R}$ denotes the chain end-to-end vector and the subscript eq the equilibrium condition. The conformation tensor is a very effective physical quantity capable of representing the overall deformed structure of short-chain polymeric systems under diverse flow fields. It is seen from Eq. (13) that at equilibrium (without flow), $\tilde{\mathbf{c}}$ is equal to the unit tensor, $\boldsymbol{\delta}$. Based on the well-known notion of a purely entropic spring force of polymer network theory,[32] we can separate temperature effects for the Lagrange multiplier (the conjugate thermodynamic field variables corresponding to $\tilde{\mathbf{c}}$), leading to a general thermodynamic expression for the internal energy function of a nonequilibrium polymeric systems under flow,

$$E = TS - PV + \mu N + Nk_BT\boldsymbol{\alpha}:\tilde{\mathbf{c}}, \tag{14a}$$

implying that[33]

$$dE = TdS - PdV + \mu dN + k_BT\boldsymbol{\alpha}:d(N\tilde{\mathbf{c}}), \tag{14b}$$

together with the extended Gibbs–Duhem thermodynamic relation.

$$-SdT + VdP - Nd\mu - N\tilde{\mathbf{c}}:d(k_BT\boldsymbol{\alpha}) = 0. \tag{14c}$$

By applying the Legendre transforms[34] to Eqs. (14a) and (14b), we can derive all other thermodynamic functions; e.g., the extended Helmholtz free energy A and Gibbs free energy G of the nonequilibrium polymeric system are

$$dA(T,V,N,N\tilde{\mathbf{c}}) = -SdT - PdV + \mu dN + k_BT\boldsymbol{\alpha}:d(N\tilde{\mathbf{c}}), \tag{15a}$$

$$A = -PV + \mu N + Nk_BT\boldsymbol{\alpha}:\tilde{\mathbf{c}}, \tag{15b}$$

and

$$dG(T,P,N,\boldsymbol{\alpha}) = -SdT + VdP + \mu dN - N\tilde{\mathbf{c}}:d(k_BT\boldsymbol{\alpha}), \tag{16a}$$

$$G = \mu N, \tag{16b}$$

respectively.

In this study, the NEMC simulations were carried out in an expanded semigrand statistical ensemble $\{N_{\mathrm{ch}}NVT\boldsymbol{\mu}^*\boldsymbol{\alpha}\}$, in which the indicated variables are held fixed:[17,33] the number of chains, N_{ch}, the average number of atoms per chain, N, the system volume V, the temperature T, the spectrum of chain relative chemical potentials, $\boldsymbol{\mu}^*$, controlling the distribution of chain lengths in the system (and thus the system polydispersity), and the thermodynamic field $\boldsymbol{\alpha}$ accounting for flow effects. The field $\boldsymbol{\alpha}$ couples with the conformation tensor $\tilde{\mathbf{c}}$ and effectively drives the system away from its equilibrium state. The corresponding probability density function in the ensemble $\{N_{\mathrm{ch}}NVT\boldsymbol{\mu}^*\boldsymbol{\alpha}\}$ is

$$\rho^{N_{\mathrm{ch}}NVT\boldsymbol{\mu}^*\boldsymbol{\alpha}}(\mathbf{r}_1,\mathbf{r}_2,\ldots,\mathbf{r}_n,V) \sim \exp\left[-\beta\left(U(\mathbf{r}_1,\mathbf{r}_2,\ldots,\mathbf{r}_n,V) - \sum_{k=1}^{N_{\mathrm{ch}}}\mu_k^*N_k - k_BT\boldsymbol{\alpha}:\sum_{k=1}^{N_{\mathrm{ch}}}\tilde{\mathbf{c}}_k\right)\right], \tag{17}$$

and thus the system configurations are sampled based on the modified Metropolis criterion,

$$p_{\mathrm{acc}}^{N_{\mathrm{ch}}NVT\boldsymbol{\mu}^*\boldsymbol{\alpha}} \sim \exp\left[-\beta\left(\Delta U - \sum_{k=1}^{N_{\mathrm{ch}}}\Delta(\mu_k^*N_k) - k_BT\boldsymbol{\alpha}:\sum_{k=1}^{N_{\mathrm{ch}}}\Delta\tilde{\mathbf{c}}_k\right)\right], \tag{18}$$

where $\beta \equiv 1/k_BT$. Here $n(=N_{\mathrm{ch}}\times N)$ is the total number of atoms in the system, $\mathbf{r}_i$ the position vector of the ith atom, U the potential energy of the system, μ_k^* the relative chemical potential of the chain of length k-mers, and $\tilde{\mathbf{c}}_k$ its conformation tensor. The uniaxial elongational flow (UEF) field was imposed in the NEMC simulations via the following form of $\boldsymbol{\alpha}$:

$$\boldsymbol{\alpha} = \begin{pmatrix} \alpha_{xx} & 0 & 0 \\ 0 & \alpha_{yy} & 0 \\ 0 & 0 & \alpha_{zz} \end{pmatrix}, \tag{19}$$

where $\alpha_{yy}=\alpha_{zz}=-\alpha_{xx}/2$. As has been shown in detail in the literature (see, e.g., Refs. 17 and 31), the Lagrange multiplier $\boldsymbol{\alpha}$ represents the external flow field and has a close relationship with the real flow field (i.e., velocity gradient tensor).

The well-known chain-connectivity altering end-bridging MC move[35] was used in the simulation in order to drive the system very efficiently to the steady state at a given value of α_{xx}. A small polydispersity index ($\approx$1.083) was chosen in conjunction with the end-bridging move. Other MC schemes [together with the end-bridging move (50%)] employed in the simulation for rigorous phase-space sampling were the reptation (10%), the end-mer rotation (2%), the flip (6%), and the concerted rotation (32%) moves.[33,35]

B. Systems studied

The polymer melt system was prepared with 160 linear $C_{78}H_{158}$ molecules in a rectangular box (enlarged in the stretching (x) direction) with the dimensions ($x\times y\times z$ in units of Angstroms) of $130.5\times54\times54$ Å^3 for the NEMD simulations of PCF and the NEMC simulations of UEF. The system for the NEMD simulations of PEF was composed of 192 $C_{78}H_{158}$ molecules in $101\times101\times45.2$ Å^3. These large box dimensions were chosen to minimize any undesirable system-size effects (especially under strong flow fields where molecules are highly stretched and oriented), based on the

fully stretched maximum chain length $|\mathbf{R}|_{max}=99.4$ Å; i.e., with the equilibrium C–C bond length (1.54 Å) and C–C–C bending angle (114°) in the all *trans*-configuration. The mean chain end-to-end distance at equilibrium is $\langle R^2\rangle_{eq}^{1/2}=38.6\pm0.8$ Å for the $C_{78}H_{158}$ melt at $T=450$ K and $\rho=0.7638$ g/cm^3. Thus, the stretching dimensions of the simulation box were at least larger than $|\mathbf{R}|_{max}$, and the other dimensions were approximately 20%–40% larger than $\langle R^2\rangle_{eq}^{1/2}$.

A broad range of strain rates were simulated corresponding to Weissenberg numbers (Wi) (defined as the product of the longest relaxation time of system, λ, and the imposed strain rate) in the interval $0.2\leq \mathrm{Wi}\leq 500$. The longest relaxation time was calculated as $\lambda=2.3\pm0.2$ ns for the $C_{78}H_{158}$ melt at $T=450$ K and $\rho=0.7638$ g/cm^3, as measured by the time integral of the stretched-exponential curve describing the autocorrelation function for the chain end-to-end vector.

For both NEMD and NEMC simulations, polymer melts were modeled by the Siepmann–Karaboni–Smit (SKS) united-atom potential model,[36] which has been widely used for simulating *n*-alkane systems under flow,[24,26] with the addition of a harmonic flexible bond-stretching potential adopted in the NEMD simulations. In order to avoid unnecessary repetition, here we present only the main features of the potential model (for details, see, for example, Refs. 24 and 36). The bond-stretching, bond-bending, bond-torsional, and interatomic LJ interactions, respectively, are given by

$$U_{str}(l)=\tfrac{1}{2}k_{str}(l-l_{eq})^2, \tag{20a}$$

$$U_{ben}(\theta)=\tfrac{1}{2}k_{ben}(\theta-\theta_{eq})^2, \tag{20b}$$

$$U_{tor}(\phi)=\sum_{m=0}^{3}a_m(\cos\phi)^m, \tag{20c}$$

and

$$U_{LJ}(r_{ij})=4\varepsilon_{ij}\left[\left(\frac{\sigma_{ij}}{r_{ij}}\right)^{12}-\left(\frac{\sigma_{ij}}{r_{ij}}\right)^{6}\right]. \tag{20d}$$

The parameter k_{str}/k_B and k_{ben}/k_B are equal to 452 900 K/Å^2 and 62 500 K/rad^2, respectively, and $a_0/k_B=1,010$ K, $a_1/k_B=2,019$ K, $a_2/k_B=136.4$ K, and $a_3/k_B=-3,165$ K. The equilibrium bond length and bond angle are $l_{eq}=1.54$ Å and $\theta_{eq}=114°$. The LJ energy and size parameters (ε/k_B and σ) are equal to (47 K and 3.93 Å) for the CH_2 united atom and (114 K and 3.93 Å) for the CH_3. For the LJ interactions between different atoms (e.g., *i* and *j*), the Lorentz–Berthelot mixing rule was employed as $\varepsilon_{ij}=(\varepsilon_i\varepsilon_j)^{1/2}$ and $\sigma_{ij}=(\sigma_i+\sigma_j)/2$. The cutoff distance of the LJ interactions used in this work was 2.5 σ_{CH2}.

IV. RESULTS AND DISCUSSION

A. NEMD simulations of simple fluids

In order to appreciate the basic aspects of the configurational temperature, we have first conducted a NEMD study of simple Weeks–Chandler–Andersen[37] (WCA) and LJ fluid systems. A total of 500 particles were used for each system. The potential models are given by[38]

$$\phi(r)=\begin{cases}4\varepsilon\left\{\left[\left(\frac{\sigma}{r}\right)^{12}-\left(\frac{\sigma}{r}\right)^{6}\right]-\left[\left(\frac{\sigma}{r_{cut}}\right)^{12}-\left(\frac{\sigma}{r_{cut}}\right)^{6}\right]\right\} & \text{for } r<r_{cut}\\ 0 & \text{for } r>r_{cut}\end{cases} \tag{21}$$

with $r_{cut}=2^{1/6}\sigma$ for the WCA model and $r_{cut}=2.5$ σ for the LJ fluid. The NEMD simulations were performed at the reduced temperature $T_{set}=0.722$ and number density $\rho=0.8442$.

In Fig. 1(a), we present the configurational temperature T_{conf} with respect to the applied (dimensionless) strain rate $\dot{\gamma}^*[=\dot{\gamma}(m\sigma^2/\varepsilon)^{1/2}]$ in PCF and PEF. At low to intermediate strain rates, no significant change in T_{conf} appears in each system [Fig. 1(a)], indicating that the system configuration is not significantly altered from the equilibrium state. With the further increase in the flow field, however, T_{conf} is observed to deviate from the set temperature, which is particularly noticeable in the systems under PEF. At a certain critical strain rate for each system, T_{conf} starts to decrease and then exhibits a sharp upturn after reaching a minimum. In addition, in each flow the WCA and LJ fluids show quantitatively very similar results to each other over the whole range of the strain rate, indicating that the overall structural changes occurring in the system induced by an external flow are not significantly different between the two potential fields; i.e., the attractive part of the LJ potential (which is missing in the WCA potential) does not seem to make a significant contribution to the overall structure. In order to see how the structural changes are reflected in the system energy, we plot in Fig. 1(b) the potential energy change ΔU (relative to the equilibrium state) versus $\dot{\gamma}^*$. Comparing to Fig. 1(a), for each system the potential energy starts to deviate from the equilibrium value at a similar critical value of $\dot{\gamma}^*$ to that for T_{conf} in Fig. 1(a) in both PCF and PEF, indicating that the structural changes are reflected consistently in both T_{conf} and ΔU. Furthermore, the critical strain rate appears to be similar to each other between the two flows.

An important observation in Fig. 1 is that all the systems exhibit a rather drastic change of ΔU after the point where the minimum of T_{conf} occurs; e.g., $\dot{\gamma}^*\approx1.5$ in PCF and $\dot{\gamma}^*\approx1$ in PEF. This change in ΔU is assumed to result from significant dynamical molecular interactions (i.e., collisions) under very strong flow fields. Based on the underlying physi-

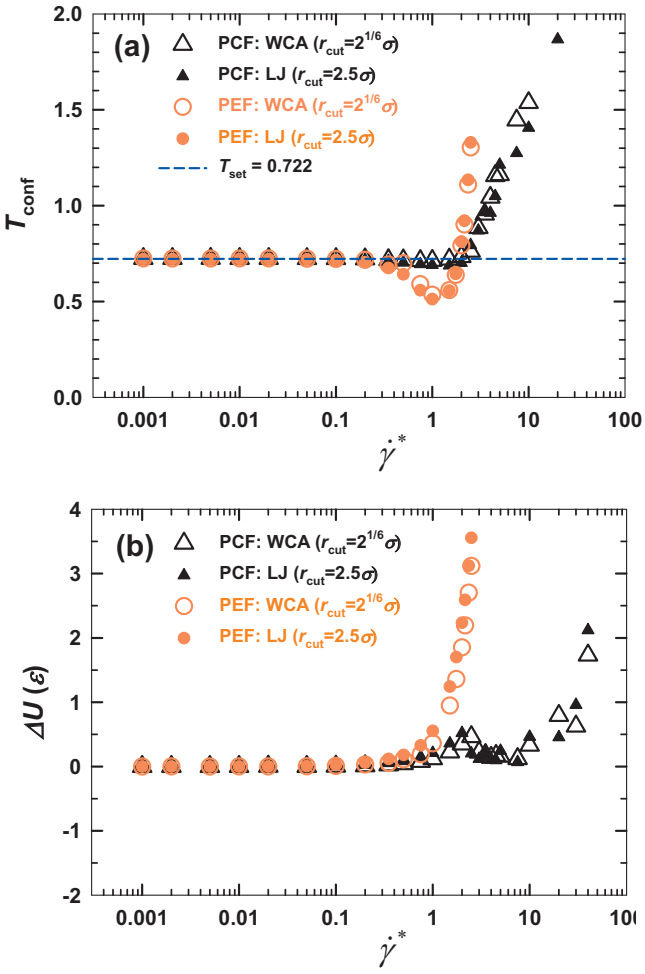

FIG. 1. Variation in (a) configurational temperature and (b) potential energy (relative to the equilibrium values) with respect to the applied (dimensionless) strain rate for simple WCA and LJ fluids under PCF and PEF at the reduced temperature $T_{set}=0.722$ and number density $\rho=0.8442$.

cal concept of the configurational temperature, we propose that T_{conf} should be taken as a physically meaningful quantity far from equilibrium only when it involves the structural (configurational) changes in the physical system without significant dynamical effects since the configurational entropy of the system should not be affected by such factors; that is, the configurational temperature should not be used in highly nonlinear regimes where the dynamical effects (the effect of molecular collisions) caused by the external flow fields become influential. (Recall that the derivation of T_{conf} was restricted to equilibrium states.[3]) We consider T_{conf} to be influenced primarily by the large-scale global structure of the system rather than the local system configuration, since the latter contribution to the total system configurational entropy is negligible compared to the large-scale structural changes. For these simple fluids, there are very small large-scale structural changes between highly nonequilibrium and equilibrium states, implying that only little contribution to T_{conf} is being provided by long-range, long timescale microstructural changes. This proposition will be critically examined when we consider polymeric materials containing various potential interaction modes, which are activated at different time and length scales.

B. NEMD simulations of polymeric fluids

Let us now turn our attention to polymeric materials. First, in Fig. 2 we display the variations in the conformation tensor components with respect to the imposed flow fields. As evident in the figure, the rotational mechanism occurring in shear flow[39] results in a much less stretched chain conformation on average (approximately up to 30% of the maximum value) than that in the planar elongational flow, where most chains have become highly stretched with increasing strain rate. Overall, the chain dimension in the stretching direction of the flow is larger in PEF than in PCF, and chains are more fully and quickly aligned to the stretching direction in PEF than in PCF, as indicated by the order parameter in Fig. 2(f).

In Fig. 3 we present the variations in the individual potential energy modes (relative to their equilibrium values) as functions of Wi in PCF and PEF. In both flows, the bond-stretching energy exhibits almost a constant value up to intermediate flow strength (i.e., $\mathrm{Wi}\leq 10$), beyond which it is observed to decrease steeply. In contrast, the bond-bending, bond-torsional, and intermolecular LJ energies initially decrease and then exhibit a marked upturn after passing a minimum. It is further noted that while the bond-torsional and intermolecular LJ energy changes become eventually positive at high strain rates in PCF, they are always negative in the case of PEF; this is due to the strong chain stretch and alignment between molecules under elongation relative to shear. This behavior directly illustrates the increasing effects of dynamical molecular interactions as the field strength increases, which was observed in simple fluids under strong flow fields. In the case of the intramolecular LJ energy, there appear some qualitative differences between the two flows, as was indicated in Fig. 2. In PCF, it increases initially and then decreases while displaying a maximum, indicating the decrease in the chain dimension beyond a critical value of flow strength. In PEF, it monotonically decreases, indicating the monotonic increase in the chain dimension. These behaviors are directly confirmed by Fig. 2(e).

We also show the separate contributions of the bonded and nonbonded energies to the total potential energy in the insets in Fig. 3. Overall, the bonded energy contribution is seen to be much larger than the nonbonded one, which is particularly obvious in PEF. Furthermore, in both flows the bond-stretching energy becomes the dominant part of the total at high flow strengths. Thus, we can expect that the bonded modes (especially, the bond stretching and the bond bending) would make a dominant contribution (especially at strong flow fields) in determining the overall value of T_{conf} via Eq. (3). As noted before, a physically meaningful T_{conf} should reflect only the large-scale structure of the system without significant dynamical (collisional) effects.

Let us now look into the configurational temperature of the polymer melt system under flow. In Fig. 4 we plot ΔT_{conf} $(=T_{conf,noneq}-T_{conf,eq})$ versus Wi. Note that the overall value of T_{conf} at low Wi is 450 K, the set point temperature. In both flows, ΔT_{conf} appears to be almost constant up to intermediate flow strength (i.e., $\mathrm{Wi}\leq 10$) and then decrease significantly with a further increase in Wi. It changes by about

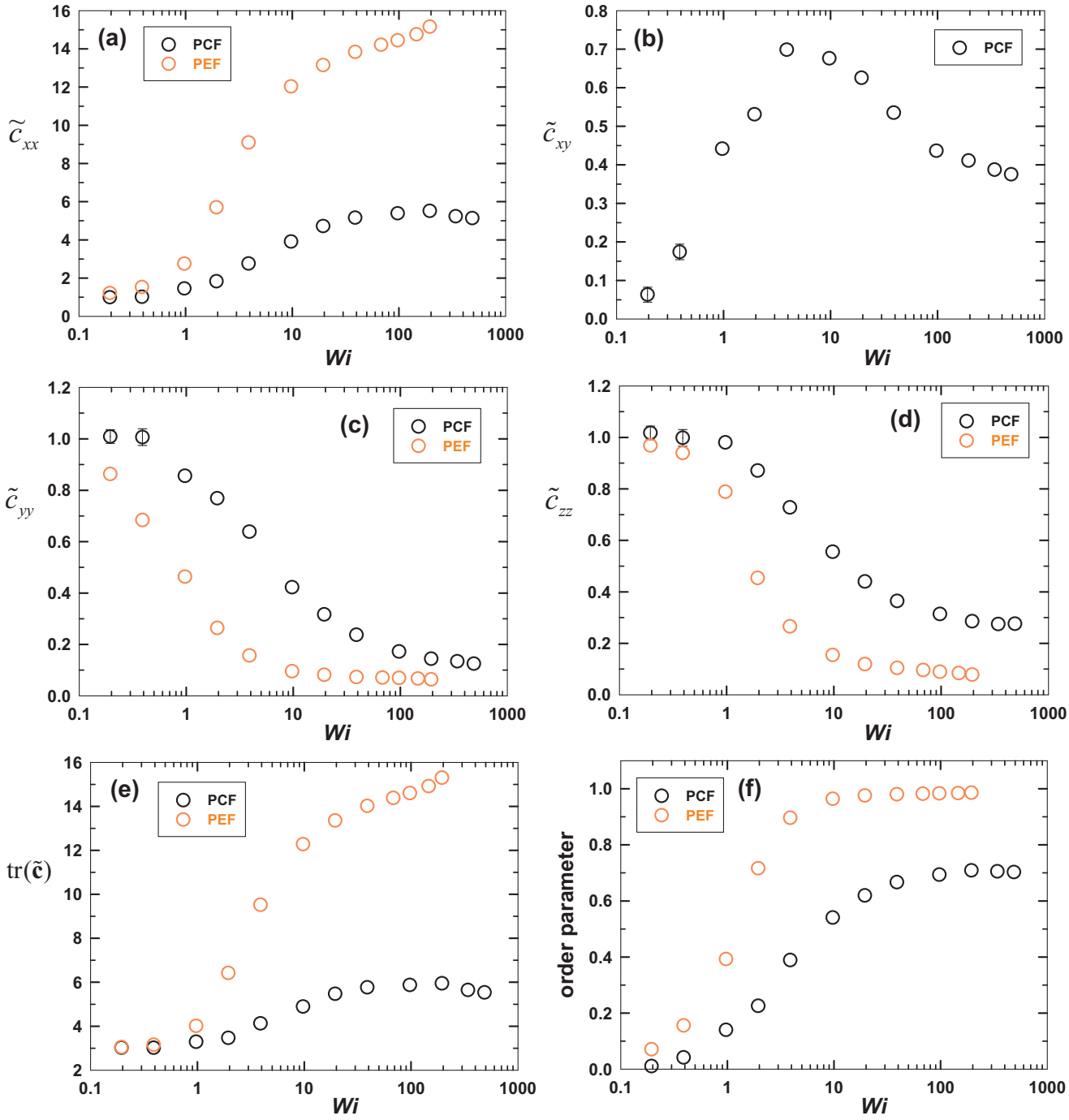

FIG. 2. [(a)–(e)] Conformation tensor components of $\tilde{\mathbf{c}}$ and (f) the order parameter as functions of Wi by NEMD simulations of $C_{78}H_{158}$ linear polyethylene melt under PCF and PEF at T=450 K and ρ=0.7638 g/cm^3. The order parameter is calculated as the largest eigenvalue of the second-rank order tensor $\mathbf{S}=\langle 3\mathbf{uu}-\boldsymbol{\delta}\rangle/2$, where $\mathbf{u}$ is the unit chain end-to-end vector.

−125 °C in PCF and −275 °C in PEF! This large variation in T_{conf} is not considered as physically reasonable in view of the structure-based configurational temperature. The origin of this behavior can be sought indirectly from the ΔU shown in Fig. 3: it is seen that not only the overall shape of the plot of ΔT_{conf} versus Wi is very similar to that of ΔU but also the incipient flow strength at which ΔT_{conf} starts to drop abruptly coincides with that of ΔU.

To see directly the source of the "aphysical" phenomenon in T_{conf}, we have analyzed separately the individual contributions of the different potential interaction modes to the configurational temperature. It is seen from Fig. 5 that the total ΔT_{conf} shown in Fig. 4 is quantitatively almost exactly the same as that of the bond-stretching mode $\Delta T_{\text{conf,str}}$. This is also obvious from the insets in Fig. 5, where the bonded part $\Delta T_{\text{conf,b}}$ and the total ΔT_{conf} are shown to superimpose. Further details have been found by separately assessing the magnitudes of $\nabla^2 U$ and $|\nabla U|^2$ involved in the calculation of T_{conf} [see Eq. (3)] for each individual interaction mode. For each quantity, the magnitude is found to vary as bond-stretching > bond-bending > bond-torsional > intermolecular LJ > intramolecular LJ. Quantitatively, the

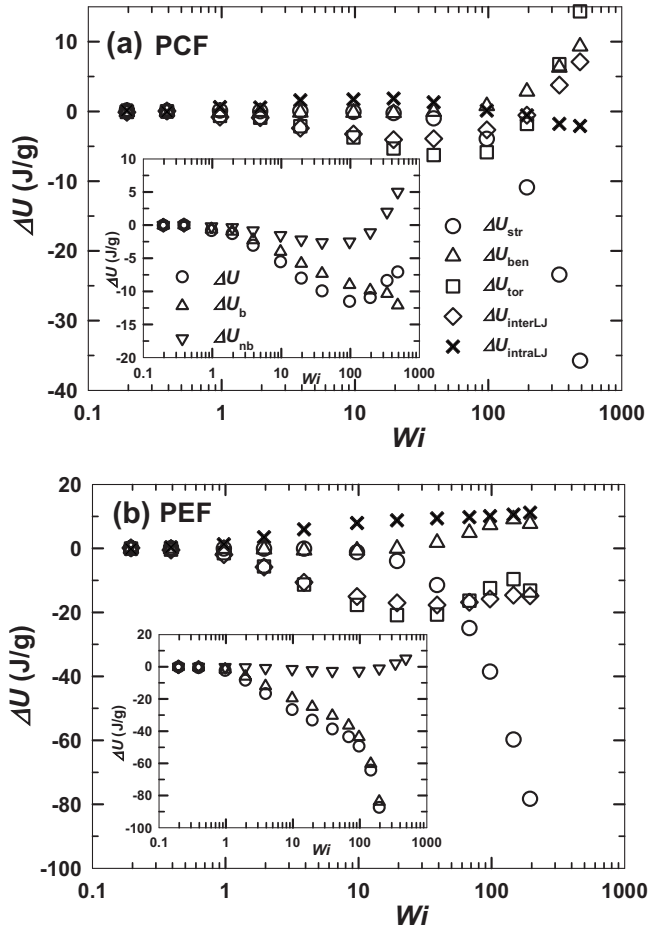

FIG. 3. Variation in the individual potential energies with respect to Wi of the $C_{78}H_{158}$ melt under (a) PCF and (b) PEF using NEMD: ΔU_{str}, bond-stretching; ΔU_{ben}, bond-bending; ΔU_{tor}, bond-torsional; $\Delta U_{interLJ}$, intermolecular LJ; $\Delta U_{intraLJ}$, intramolecular LJ; ΔU_b, the bonded modes (bond-stretching, bond-bending, and bond-torsional); ΔU_{nb}, the nonbonded modes (intermolecular and intramolecular LJ); ΔU, the total.

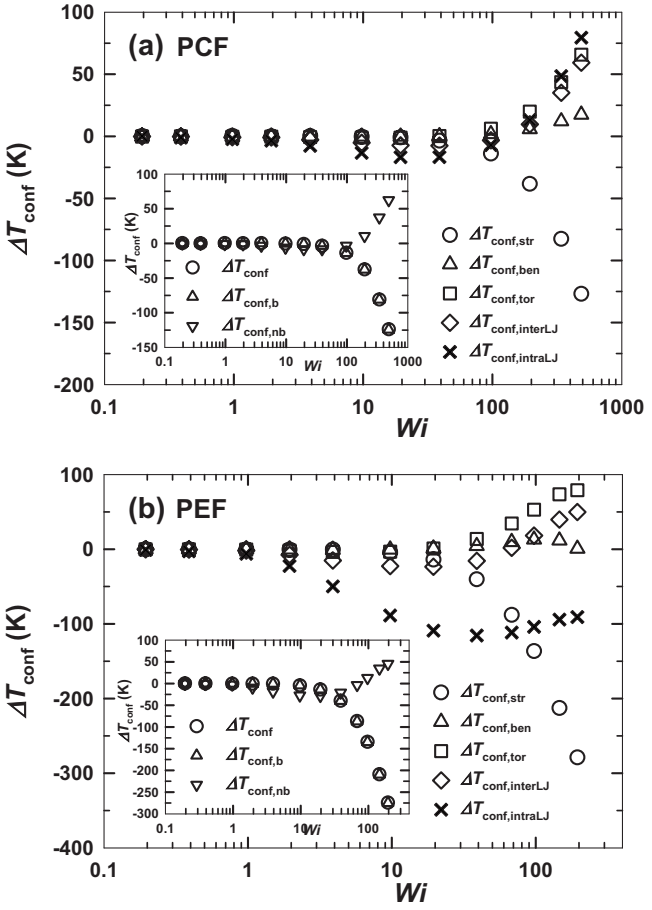

FIG. 5. Plots of ΔT_{conf} vs Wi for each individual potential interaction mode based on Eq. (4) for (a) PCF and (b) PEF using NEMD: $\Delta T_{conf,str}$, bond-stretching; $\Delta T_{conf,ben}$, bond-bending; $\Delta T_{conf,tor}$, bond-torsional; $\Delta T_{conf,interLJ}$, intermolecular LJ; $\Delta T_{conf,intraLJ}$, intramolecular LJ; $\Delta T_{conf,b}$, the bonded modes (bond-stretching, bond-bending, and bond-torsional); $\Delta T_{conf,nb}$, the nonbonded modes (intermolecular and intramolecular LJ); ΔT_{conf}, the total.

bond-stretching contribution is almost one order of magnitude (i.e., nine to ten times) larger than the bond-bending contribution, which is in turn approximately one order of magnitude (i.e., approximately ten times) larger than the bond-torsional contribution. The intermolecular LJ contribution is about four times smaller than the bond-torsional and about five times larger than the intramolecular LJ contribution. Thus, the total bonded contribution (mostly the bond-stretching and bond-bending modes) to $\nabla^2 U$ and $|\nabla U|^2$ turns out to be about 300 times larger than the total nonbonded one. This explains why the total ΔT_{conf} is practically the same as the bonded part ($\Delta T_{conf,b}$), irrespective of the nonbonded part ($\Delta T_{conf,nb}$). Furthermore, $\Delta T_{conf,str}$ is quantitatively very close to ΔT_{conf}; i.e., the bond-stretching (≈86.5%), bond-bending (≈11.8%), bond-torsional (≈1.2%), nonbonded intermolecular (≈0.4%), and intramolecular (≈0.1%) LJ in $\nabla^2 U$ and $|\nabla U|^2$. Similarly, it is to be expected that by neglecting (or freezing) the bond-stretching mode (as in the original SKS model[36]), the bond-bending contribution would dominate over all the other modes and thus determine the total ΔT_{conf} which, according to the result in Fig. 5, is now increasing with the flow strength. This behavior was also observed by Delhommelle-Evans[14] in their NEMD study of *n*-decane with constrained bond length.

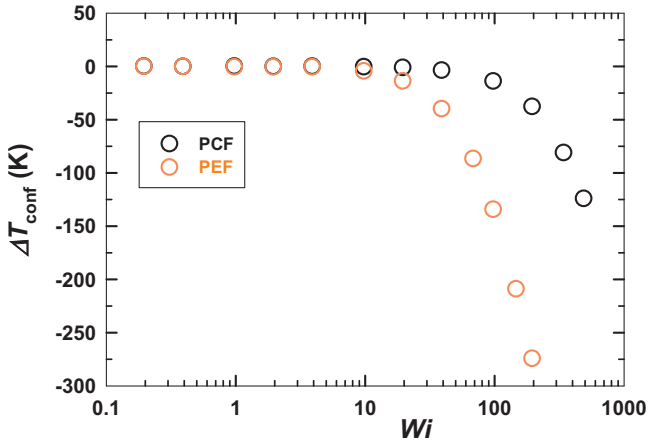

FIG. 4. Plots of ΔT_{conf} ($=T_{conf,noneq}-T_{conf,eq}$) vs Wi of the $C_{78}H_{158}$ melt using NEMD where ΔT_{conf} denotes the configurational temperature change relative to the equilibrium value.

As an interesting point, we note that even at equilibrium, T_{conf} of each individual interaction mode may be different from the imposed set temperature; that is, in the equilibrium MD simulation of $C_{78}H_{158}$ melt at $T=450$ K, it is found that $T_{conf,str}=450.6\pm0.3$ K, $T_{conf,ben}=450.4\pm0.4$ K, $T_{conf,tor}$

$=473.8\pm0.5$ K, $T_{conf,interLJ}=394.5\pm0.8$ K, and $T_{conf,intraLJ}=396\pm2.4$ K, indicating the existence of the cross correlations between different interaction modes. Similar results are also observed in the equilibrium MC simulation. The differences between the set temperature and the configurational temperature represented separately by the bond-torsional and the nonbonded modes reflect the existence of the dynamical correlations between different modes (here the bond-stretching and bond-bending modes are to be almost not affected by such correlation effects due to their very strong and fast dynamic response). We further conjecture that an external flow field might lead to some changes (but presumably not very large) relative to the equilibrium state in the degree of the correlations among different interaction modes, especially for slow interaction modes as the flow field is likely to change (e.g., decrease) the apparent time scales of the response of those modes.

For a further analysis, we first note that due to their very strong interaction potential, the bond-stretching and bond-bending modes are very fast in time scale and rapidly equilibrated around their equilibrium values with small fluctuations, not only at equilibrium but also for nonequilibrium states, in general. However, such strong potentials make even a small increase in the fluctuations caused by significant molecular collisions under strong flow fields to produce a huge impact on the overall T_{conf}. Such large dynamical effects should not be included in the calculation of a physically meaningful T_{conf}, since it cannot represent or incorporate those effects from the thermodynamic viewpoint (i.e., the configurational entropy does not accommodate such factors). Furthermore, the main difference between equilibrium and nonequilibrium states for polymeric systems generally lies in the change in the overall (global) structure; i.e., the local, very short structure (represented by the bond-stretching and bond-bending modes) is barely changing between equilibrium and nonequilibrium states, and its contribution to the total system configurational entropy is negligible compared to the large-scale structural changes (represented by the bond-torsional and nonbonded modes). Based on these facts, we thus neglect the contribution to the total change in T_{conf} by the local interaction modes (the bond-stretching and bond-bending), which hardly affect the global structure of the system. Indeed, the potentials for these models were determined under equilibrium conditions, and any significant changes in them for highly nonequilibrium states is likely an artifact of the model potentials rather than an experimentally observed phenomenon; i.e., in reality one would not expect such large fluctuations from the equilibrium bond distance and bond angle as were present in the simulations.

In Fig. 6(a) we present the plot of $\Delta T_{conf,(tor+nb)}$ versus Wi in which only the bond-torsional and the non-bonded LJ interaction modes are included in the calculation of T_{conf}. Note that these modes fluctuate on a much longer timescale than the bond-stretching and bond-bending modes. In both flows, $\Delta T_{conf,(tor+nb)}$ is observed to initially decrease (more clearly seen in the inset) as Wi increases, but then increases dramatically with a further increase in the flow strength with the presence of a minimum (located approximately $5\leq Wi\leq10$). Qualitatively similar behavior is also observed for the

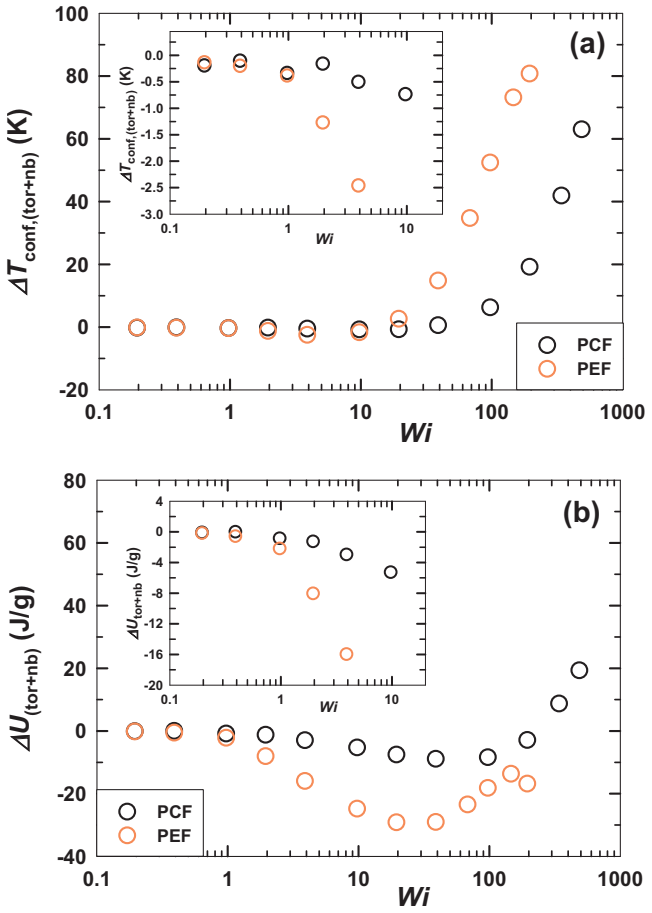

FIG. 6. Plots of (a) $\Delta T_{conf,(tor+nb)}$ and (b) $\Delta U_{(tor+nb)}$ vs Wi under PCF and PEF using NEMD, including only the bond-torsional and the nonbonded LJ contributions.

corresponding potential energy $\Delta U_{(tor+nb)}$, as shown in Fig. 6(b), although the location of the minimum for each flow occurs at a larger Wi value in case of $\Delta U_{(tor+nb)}$ than $\Delta T_{conf,(tor+nb)}$. This indicates the higher sensitivity to the flow strength of the first and the second derivatives of the potential energy involved in $\Delta T_{conf,(tor+nb)}$ than the potential energy itself.

As is well known from experiment, linear polyethylenes typically exhibit more ordered structures (i.e., chains are stretched and aligned with each other) as the temperature decreases and can be crystallized at low temperatures. From a thermodynamic viewpoint, this occurs as a result of the relative increase in the energetic effect over the entropic one on the system structure with decreasing temperature.[40,41] Alternatively, such ordered structures can also be induced by subjecting the system to an external flow field. Assuming T_{conf} to represent the overall structure of polyethylene systems, it is therefore physically reasonable to expect that ΔT_{conf} of the system would generally be negative under an external flow field as it induces the ordering of the system structure. Hence, we consider the sharp upturn of $\Delta T_{conf,(tor+nb)}$ at certain critical Wi shown in Fig. 6(a) to be a physically unrealistic phenomenon caused by the significant influence of molecular collisions at strong flow fields where T_{conf} is likely to lose its original meaning. This is likely a consequence of the definition of T_{conf}, which relies on a local

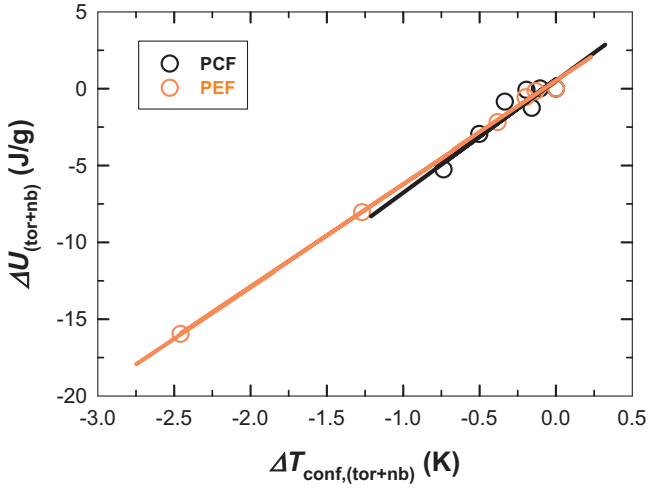

FIG. 7. Plots of $\Delta U_{(\mathrm{tor+nb})}$ vs $\Delta T_{\mathrm{conf},(\mathrm{tor+nb})}$ for PCF and PEF in NEMD. The solid lines represent the linear fits.

or quasiequilibrium expression of the entropy. Thus, in order to obtain a physically meaningful T_{conf} that accurately describes the structural changes occurring in nonequilibrium states, the dynamical effects exhibited by the interaction modes should be excluded, as the configurational entropy of the system would not be affected by such factors. This assertion is further supported below and later when we analyze the NEMC data with comparison to the NEMD results.

In Fig. 7 we plot $\Delta U_{(\mathrm{tor+nb})}$ versus $\Delta T_{\mathrm{conf},(\mathrm{tor+nb})}$ for both flows, only including the data up to the minima in Fig. 6. It is evident that the data set from each flow is well represented by a linear plot. Furthermore, the slopes from PCF and PEF are found to be remarkably close to each other, implying the physical consistency conferred by the configurational temperature in regard to its representation of the overall system structure. We also note that in the regime shown in Fig. 7, $\Delta U_{(\mathrm{tor+nb})}$ is found to be almost the same as the total ΔU (i.e., $\Delta U_{(\mathrm{tor+nb})}$ amounts to about 95% of ΔU), indicating very little change in the bond-stretching and bond-bending energies, which we have already stated should not change much with increasing Wi. The slope of ΔU versus $\Delta T_{\mathrm{conf},(\mathrm{tor+nb})}$, only including the data at low strain rates near the equilibrium state (i.e., ΔU and $\Delta T_{\mathrm{conf},(\mathrm{tor+nb})} \ll 1$) plus the kinetic contribution $[\approx 0.89\ \mathrm{J/(g\ K)}]$, is calculated as $2.5 \pm 1.1\ \mathrm{J/(g\ K)}$ for PCF and $2.7 \pm 1.3\ \mathrm{J/(g\ K)}$ for PEF. It is interesting that these values turn out to be very close to the experimental heat capacity[42] of amorphous polyethylene of 2.67 J/(g K) at $T=450$ K. This result might have been expected to some extent from the fluctuation-dissipation theorem of linear irreversible thermodynamics, which states that the dynamical mechanisms occurring strictly at equilibrium states are to be exactly the same as those occurring under nonequilibrium conditions, as long as the applied external perturbations are sufficiently small compared to intrinsic thermal Brownian effects. Accordingly, the nonequilibrium heat capacity represented by the system energy change with respect to the change in the configurational temperature, which is in turn caused by the change in the overall, large-scale system structure due to sufficiently small external perturbations (flow fields), can be related to the equilibrium heat capacity represented by the energy change with respect to the system temperature at equilibrium states. The present analysis shows that the nonequilibrium heat capacity found in this way converges quantitatively to the equilibrium heat capacity, under very weak external flow fields, implying that near equilibrium, the structural change caused by weak external fields (directly reflected in ΔT_{conf}) could also be generated by varying the equilibrium temperature.

C. NEMC simulations of polymeric fluids

Let us now look into the results from the NEMC simulations of UEF, where the temperature is naturally imposed via the probability density function based solely on the positions of atoms. Therefore, such large dynamical effects on the configurational temperature (and the potential energy) present in NEMD simulations at strong flow fields are absent in the MC results. This further implies a potential consistency between the NEMC and NEMD data for ΔT_{conf} in the regime where dynamical interactions are weak. Furthermore, in the NEMC simulations the bond-stretching energy has been removed, as in the original SKS model.[36]

In Fig. 8 we present the conformation tensor components as functions of the field strength. As expected, with increasing the field, $\tilde{c}_{xx}$ ($\tilde{c}_{yy}$ and $\tilde{c}_{zz}$) appears to increase (decrease) steeply, especially in the intermediate range of α_{xx} ($0.3 \leq \alpha_{xx} \leq 0.6$). These results are seen to be consistent with the NEMD results of PEF (Fig. 2). In addition, by comparing to the NEMD result of PEF for the conformation tensor, we roughly estimate the range of the field strength imposed by α_{xx} in the NEMC simulations as approximately close to that of the NEMD of PEF.

Figure 9(a) presents the potential energy change in each individual interaction mode. The monotonic increase in the intramolecular LJ energy is (quantitatively) similar to that observed in the NEMD simulation of PEF. However, the bond-bending energy exhibits very little change even at high field strengths; this indicates the absence of a contribution by dynamic molecular collisions in the MC simulations, as opposed to the NEMD. Furthermore, in contrast to the PEF NEMD result [Fig. 3(b)], the bond-torsional and the intermolecular LJ energies are observed to monotonically decrease with the field strength without showing a minimum, again indicating the absence of molecular collisions in the MC method. Also shown in Fig. 9(a) is the monotonic decrease in the nonbonded potential energy, as again contrasting with the concave behavior shown in the NEMD simulations of PEF. Furthermore, although the bonded energy as well as the total energy is shown to decrease monotonically in the NEMC simulations, apparently similar to the PEF NEMD simulations, the main sources are very different from each other. In other words, whereas in the NEMC simulations the overall decrease in the bonded energy results primarily from the decrease in the bond-torsional energy as the molecules become more stretched with increasing the field, in the NEMD it is mostly caused by the aphysically large decrease in the bond-stretching energy [see Fig. 3(b)].

Also shown in Fig. 9(a) is the field energy change $\Delta U_{\mathrm{field}}$ $(=N_{\mathrm{ch}} k_B T \boldsymbol{\alpha}:\tilde{\mathbf{c}})$ which monotonically increases with the field

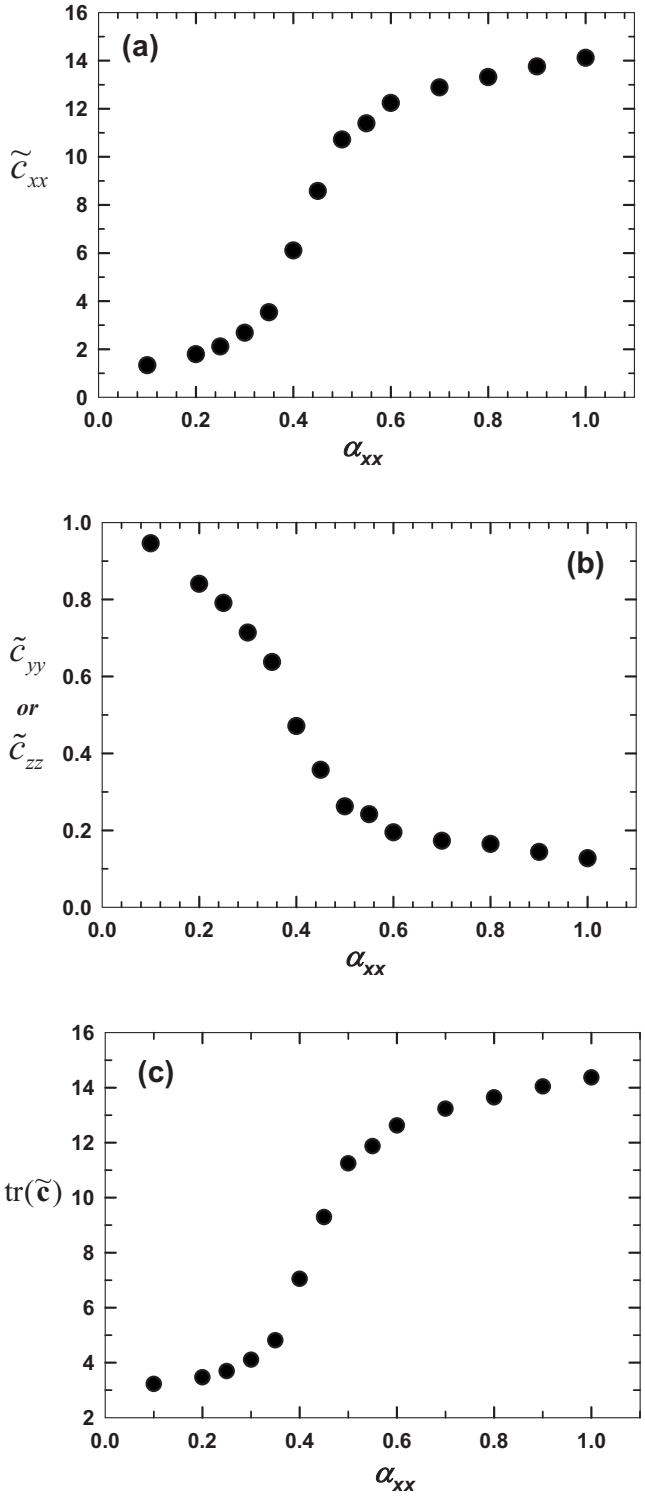

FIG. 8. Plot of the conformation tensor components of $\tilde{\mathbf{c}}$ as functions of the field strength α_{xx} from NEMC simulations of the $C_{78}H_{158}$ liquid under UEF.

strength as the chains become more stretched. Further thermodynamic information of the field effect can be obtained by calculating $N_{ch}k_BT\int_0^{\boldsymbol{\alpha}}\tilde{\mathbf{c}}:d\boldsymbol{\alpha}$ via thermodynamic integration [as referred to Eqs. (15) and (16)], which enables us to calculate the free energy change at nonequilibrium states.[44]

The effects of the field on the configurational temperature are shown in Fig. 9(b). In contrast to the NEMD simulations, the bond-bending mode $\Delta T_{conf,ben}$ shows a very small value even at strong fields where the system structure is evi-

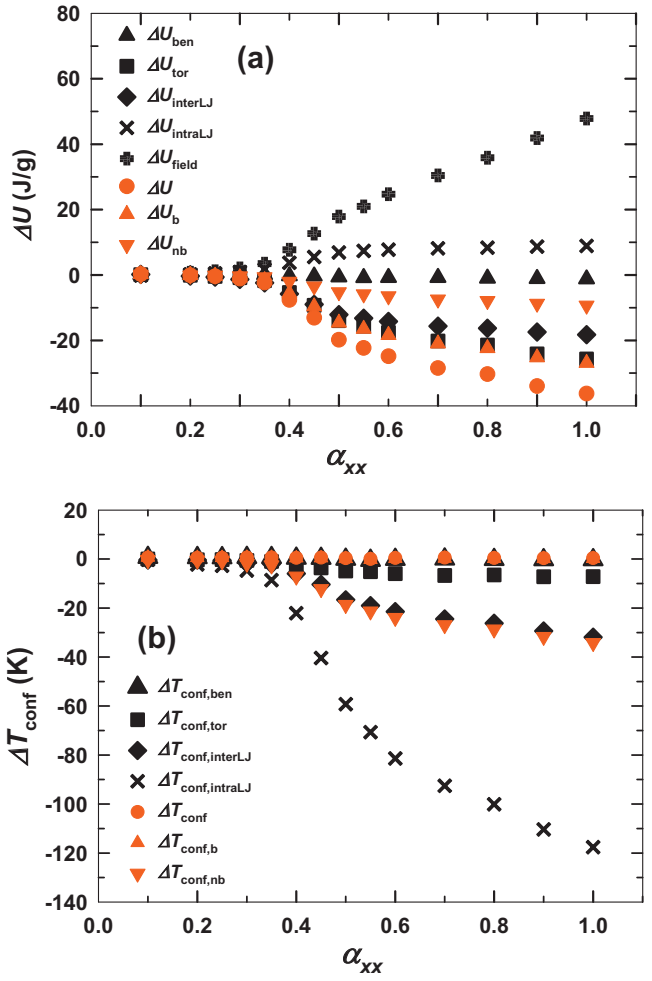

FIG. 9. Variation in (a) the potential energy ΔU and (b) the configurational temperature ΔT_{conf} for the individual interaction modes with respect to α_{xx}. The same notations for the subscripts as in Fig. 5 are used. The field energy change ΔU_{field} is calculated as $N_{ch}k_BT\boldsymbol{\alpha}:\tilde{\mathbf{c}}$ [see Eq. (14a)].

dently highly deformed. This demonstrates again an "artificial" change in $\Delta T_{conf,ben}$ caused by molecular collisions in the NEMD simulations at strong flow fields. In contrast, the bond-torsional ($\Delta T_{conf,tor}$), intermolecular ($\Delta T_{conf,interLJ}$), and intramolecular LJ ($\Delta T_{conf,intraLJ}$) modes are observed to decrease monotonically over the whole range of α_{xx}. A particularly noticeable change appears in the intramolecular LJ mode, reflecting a highly deformed chain configuration. An important observation is that these three modes in the MC simulations are quantitatively consistent with those observed in the NEMD simulations of PEF [Fig. 5(b)] within the intermediate range of the flow field (i.e., $Wi \leq 10$), where dynamical artifacts in ΔT_{conf} are assumed to be relatively small. Another important point in Fig. 9(b) is that the total ΔT_{conf} is quantitatively almost the same as $\Delta T_{conf,ben}$ and $\Delta T_{conf,b}$, as in the NEMD simulations. We have confirmed that this behavior again originates from the large differences between the interaction modes in the magnitudes of $\nabla^2 U$ and $|\nabla U|^2$. The relative magnitudes between the interactions are found to be quite similar to those found in the NEMD simulations.

In Fig. 10 we plot $\Delta T_{conf,(tor+nb)}$ and $\Delta U_{(tor+nb)}$ as functions of α_{xx}. These two quantities exhibit a very similar (physically consistent) behavior to each other and are quali-

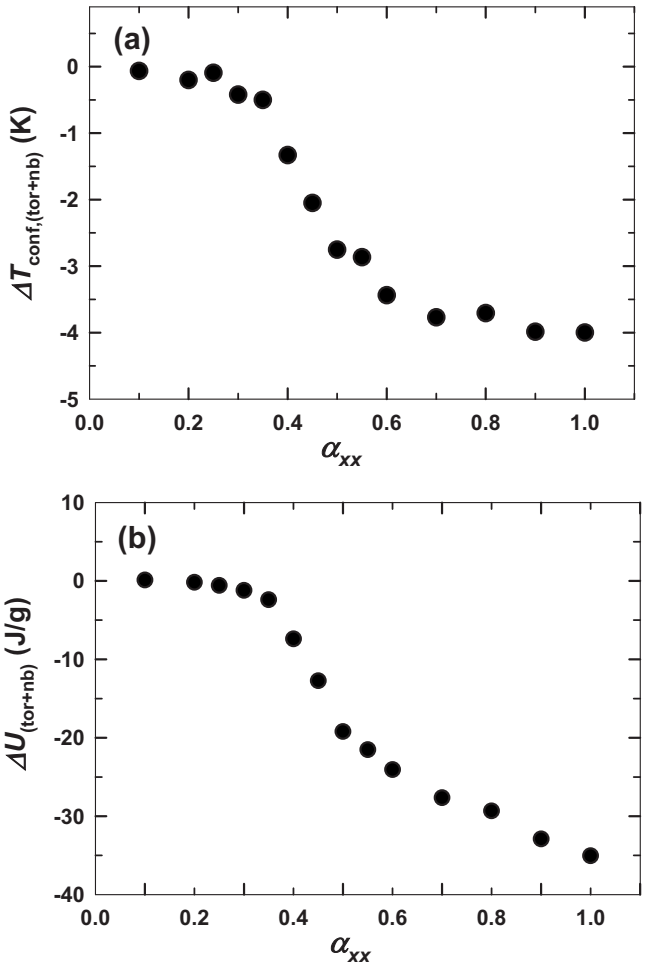

FIG. 10. Plots of (a) $\Delta T_{conf,(tor+nb)}$ and (b) $\Delta U_{(tor+nb)}$ vs α_{xx}, including only the bond-torsional and the nonbonded LJ contributions.

tatively consistent with the NEMD result shown in Fig. 6: Only within the intermediate flow strengths ($Wi \leq 10$), where the dynamical artifacts of NEMD simulations are relatively small in T_{conf}, are the two simulations found to be fully consistent with each other.

Lastly, we present the plot of $\Delta U_{(tor+nb)}$ versus $\Delta T_{conf,(tor+nb)}$ from the NEMC simulations in Fig. 11 where we also include the NEMD data of both PCF and PEF presented in Fig. 7. It is clearly seen that the NEMC and NEMD data are quantitatively consistent with each other; here, however, we should notice that all the NEMC data in the whole range of α_{xx} are included in the figure, while only NEMD data are presented in the restricted range of Wi. This result further corroborates our hypothesis that the configurational temperature would maintain a sound physical basis only by reflecting the large-scale structural changes in the system without an artificial dynamical contribution, which dominates at strong flow fields in NEMD simulations. Furthermore, although the original derivation of T_{conf} was limited to equilibrium states, excluding the fast timescale interaction modes (stretching and bending) thus seems to be consistent with the hypothesis of extended local or quasiequilibrium that is usually assumed in nonequilibrium thermodynamics theory.[18,22,23]

The slope of the plot of $\Delta U_{(tor+nb)}$ versus $\Delta T_{conf,(tor+nb)}$

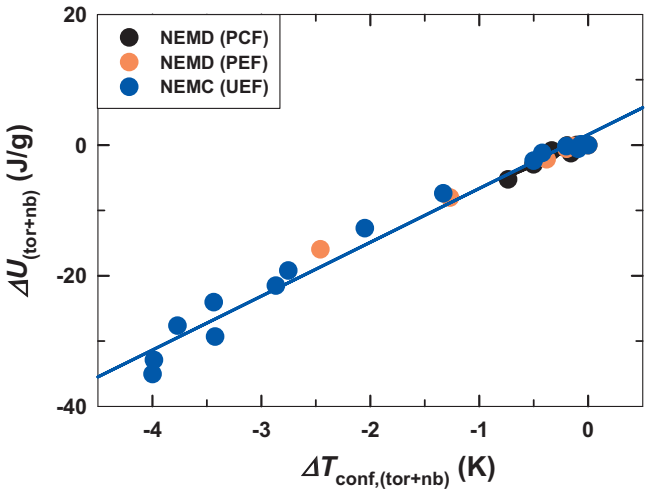

FIG. 11. Plots of $\Delta U_{(tor+nb)}$ vs $\Delta T_{conf,(tor+nb)}$ from NEMC simulations. Also shown are the NEMD data of PCF and PEF for comparison. The solid line represents the linear fit of the NEMC data.

using the data near equilibrium is calculated as 2.75 ± 0.99 J/(g K), which is also consistent with the NEMD result [2.5 ± 1.1 J/(g K) for PCF and 2.7 ± 1.3 J/(g K) for PEF] and the experimental value[42] of 2.67 J/(g K). It has been further demonstrated in a recent NEMC simulation study[43,44] of the flow-induced polymer crystallization under strong flow fields that the application of $\Delta T_{conf,(tor+nb)}$ correctly discerns the flow-induced crystalline phase from the simple oriented melt and even quantitatively predicts remarkably well the flow-enhanced melting-point elevation that has been reported in experiment. Furthermore, inclusion of data at higher flow strengths might enable calculation of a nonequilibrium heat capacity.[44]

V. CONCLUSIONS

We have presented a thorough analysis of the characteristics of the configurational temperature (T_{conf}) using both NEMD and NEMC simulations of $C_{78}H_{158}$ linear polyethylene melts under shear and elongational flows. The NEMD simulations exhibited a dramatic decrease in T_{conf} at strong flow fields ($Wi \geq 20$). Such a large degree of reduction in T_{conf} in NEMD is considered physically unrealistic, resulting from the significant effects of the dynamical molecular interactions (especially exhibited by the bond-stretching and bond-bending modes). A separate analysis of the individual contributions from the different potential interaction modes to the configurational temperature has revealed that the bonded modes (particularly the bond-stretching and bond-bending modes) make a dominant contribution over the nonbonded ones and thus determine the overall T_{conf}. The quantitative analysis of the individual contributions to $\nabla^2 U$ and $|\nabla U|^2$ involved in the calculation of T_{conf} showed that bond-stretching($\approx 86.5\%$) > bond-bending($\approx 11.8\%$) > bond-torsional($\approx 1.2\%$) > the intermolecular LJ($\approx 0.4\%$) > the intramolecular LJ($\approx 0.1\%$). Therefore, the bond-stretching contribution is almost one order of magnitude (i.e.,

nine to ten times) larger than the bond-bending contribution, which is about one order of magnitude (i.e., approximately ten times) larger than the bond-torsional contribution. The intermolecular LJ contribution is about four times smaller than the bond-torsional, but about five times larger than the intramolecular LJ contribution. Because of this, T_{conf} in NEMD was observed apparently to match the bond-stretching mode ($T_{\text{conf,str}}$), as shown in Fig. 5. Furthermore, if we neglect the bond-stretching mode, the bond-bending mode (the second largest contribution) would comprise the dominant contribution and determine the total T_{conf}, leading to the overall increase in T_{conf} with increasing flow strength in both PCF and PEF; this is consistent with the observations of Delhommelle-Evans[14] in their NEMD study of an *n*-decane system with constrained bond length.

Such dramatic and nonmonotonic changes in T_{conf} of each individual mode observed in the NEMD simulations due to the influence of strong dynamic molecular collisions under strong flow fields were not observed in the NEMC simulations (compare Figs. 5 and 9). Based on the physical concept of the configurational temperature associated with the structural changes in the system, we hypothesized that such dynamical effects should not be included in the calculation of T_{conf}. Furthermore, as the bond-stretching and bond-bending modes experience very fast fluctuations of short timescales and rapidly equilibrate around their equilibrium values and are associated with only the local structure of the chains, in order to describe accurately the structural changes occurring at nonequilibrium states by use of the configurational temperature we propose to exclude their contributions in calculating the change in T_{conf} between equilibrium and highly nonequilibrium states (as ΔT_{conf} should reflect mainly the large-scale structural and long timescale changes of the system) and thus only the bond-torsional and nonbonded modes are taken into account to generate a physically meaningful ΔT_{conf}.

This proposition (excluding the bond-stretching and bond-bending modes, and excluding the dynamical effects in obtaining a physically meaningful ΔT_{conf} between equilibrium and nonequilibrium states) is supported by good agreement between the NEMC and NEMD simulations when we only include the NEMD data within the intermediate range of strain rates where dynamical effects are relatively suppressed (see Fig. 11). Under this hypothesis, the NEMD results between PCF and PEF are shown to be consistent with each other (see Fig. 7). Further evidence arises from the fact that $\Delta T_{\text{conf,(tor+nb)}}$ predicts remarkably well the experimental heat capacity of amorphous polyethylene melts[42] and the melting-point elevation under flow.[43,44]

The general features revealed from the present work are expected to be valid for other polymeric systems as well, although the specific quantitative aspects may be different for various materials as they are characterized by different potentials and force fields. We anticipate that the present study would be useful in the application of the configurational temperature for interpreting many other physical phenomena (e.g., phase separation or transitions in polymeric systems) as well as flowing polymeric materials.

ACKNOWLEDGMENTS

This work was supported by the National Science Foundation under Grant No. CBET-0742679, and used the resources of the PolyHub Virtual Organization.

APPENDIX A: CONFIGURATIONAL TEMPERATURE IN A GENERALIZED CANONICAL ENSEMBLE

In order to derive a generalized expression for the configurational temperature for the systems under an arbitrary set of external thermodynamic fields, as suggested by Ilg,[45] we start from the generalized canonical ensemble[23] which accounts for a complete set of the thermodynamic state variables and the conjugate thermodynamic fields (Lagrange multipliers $\boldsymbol{\lambda}$). The probability density function $\rho_{[\boldsymbol{\lambda}]}$ under the conditions of $[\boldsymbol{\lambda}]$ in this ensemble can be written as

$$\rho_{[\boldsymbol{\lambda}]}(\boldsymbol{\Gamma}) = \frac{1}{Q(\boldsymbol{\lambda})}\exp\left(-\beta H(\boldsymbol{\Gamma}) - \sum_k \lambda_k \Pi_k(\boldsymbol{\Gamma})\right), \tag{A1}$$

$$Q(\boldsymbol{\lambda}) = \int \exp\left(-\beta H(\boldsymbol{\Gamma}) - \sum_k \lambda_k \Pi_k(\boldsymbol{\Gamma})\right) d\boldsymbol{\Gamma}, \tag{A2}$$

where $\beta \equiv 1/k_B T$, $\boldsymbol{\Gamma}$ represents the full phase-space consisting of all the N-particle positions ($\mathbf{r}$) and momenta ($\mathbf{p}$) in the system, and $Q(\boldsymbol{\lambda})$ is the corresponding partition function of this ensemble. We first write the statistical-mechanical expression for the average of the sum of the square of the force acting on each particle ($\mathbf{F}_i = -\boldsymbol{\nabla}_i U$),

$$\left\langle \sum_{i=1}^{N} \mathbf{F}_i^2 \right\rangle = \int d\mathbf{z}\rho_{[\boldsymbol{\lambda}]}(\boldsymbol{\Gamma}) \sum_{i=1}^{N} \mathbf{F}_i^2. \tag{A3}$$

Substituting Eqs. (A1) into Eq. (A2), we then obtain

$$\left\langle \sum_{i=1}^{N} \mathbf{F}_i^2 \right\rangle = \frac{1}{Q(\boldsymbol{\lambda})} \int d\boldsymbol{\Gamma} \left(\sum_{i=1}^{N} \boldsymbol{\nabla}_i U \cdot \boldsymbol{\nabla}_i U \right) \times \exp\left(-\beta H(\boldsymbol{\Gamma}) - \sum_k \lambda_k \Pi_k(\boldsymbol{\Gamma})\right), \tag{A4}$$

which can be rewritten as

$$\left\langle \sum_{i=1}^{N} \mathbf{F}_i^2 \right\rangle = \frac{1}{Q(\boldsymbol{\lambda})} \int d\boldsymbol{\Gamma} \sum_{i=1}^{N} \boldsymbol{\nabla}_i U \cdot \left\{ -\beta^{-1} \left[\boldsymbol{\nabla}_i \exp\left(-\beta H - \sum_k \lambda_k \Pi_k\right) + \left(\sum_k \lambda_k \boldsymbol{\nabla}_i \Pi_k\right) \times \exp\left(-\beta H - \sum_k \lambda_k \Pi_k\right) \right] \right\}. \tag{A5}$$

Separately evaluating the two terms in Eq. (A5), we arrive at

$$\left\langle \sum_{i=1}^{N} \mathbf{F}_i^2 \right\rangle = \beta^{-1} \left\langle \sum_{i=1}^{N} \boldsymbol{\nabla}_i^2 U \right\rangle - \beta^{-1} \left\langle \sum_{i=1}^{N} \left(\boldsymbol{\nabla}_i U \cdot \sum_k \lambda_k \boldsymbol{\nabla}_i \Pi_k \right) \right\rangle. \tag{A6}$$

Rearranging Eq. (A6) for the temperature, we finally obtain a

generalized expression for the configurational temperature as[45]

$$\frac{1}{k_B T_{\text{conf}}} = -\frac{\langle \Sigma_{i=1}^{N} \nabla_i \cdot \mathbf{F}_i \rangle - \langle \Sigma_{i=1}^{N} (\mathbf{F}_i \cdot \Sigma_k \lambda_k \nabla_i \Pi_k) \rangle}{\langle \Sigma_{i=1}^{N} \mathbf{F}_i^2 \rangle}. \quad \text{(A7)}$$

In our present NEMC simulations, the additional thermodynamic structural variable $\mathbf{\Pi}$ and the corresponding Lagrange multiplier $\boldsymbol{\lambda}$ are set equal to $\Sigma_{l=1}^{N_{\text{ch}}} \tilde{\mathbf{c}}_l$ and $-\boldsymbol{\alpha}$, respectively. Equation (A7) is thus reduced to

$$\frac{1}{k_B T_{\text{conf}}} = -\frac{\langle \Sigma_{i=1}^{n} \nabla_i \cdot \mathbf{F}_i \rangle + \boldsymbol{\alpha} : \langle \Sigma_{i=1}^{n} (\mathbf{F}_i \cdot (\nabla_i \Sigma_{l=1}^{N_{\text{ch}}} \tilde{\mathbf{c}}_l)) \rangle}{\langle \Sigma_{i=1}^{n} \mathbf{F}_i^2 \rangle}$$

$$= -\frac{\langle \Sigma_{i=1}^{n} \nabla_i \cdot \mathbf{F}_i \rangle + \boldsymbol{\alpha} : \Sigma_{l=1}^{N_{\text{ch}}} \frac{6(\mathbf{F}_{l,N_l} - \mathbf{F}_{l,1}) \mathbf{R}_l}{\langle R^2(N_l) \rangle_{\text{eq}}}}{\langle \Sigma_{i=1}^{n} \mathbf{F}_i^2 \rangle}, \quad \text{(A8)}$$

where $\mathbf{R}_l$ is the chain end-to-end vector of the lth-chain and $\langle R^2(N_l) \rangle_{\text{eq}}$ denotes the mean-square chain end-to-end distance of length N_l-mers at equilibrium. $\mathbf{F}_{l,1}$ and $\mathbf{F}_{l,N_l}$ are the forces acting on the first atom and the last atom, respectively of the lth-chain. Since the force acting on an atom is statistically random and furthermore only the two end atoms are involved, the additional field term in the numerator of Eq. (A8) is supposed to make a negligible contribution.

APPENDIX B: DERIVATION OF THE FORMULA OF $\nabla \cdot \mathbf{F}$

In this appendix, we derive the analytical formula of $\nabla \cdot \mathbf{F}$ involved in the calculation of the configurational temperature [Eq. (4)] for each potential interaction type. For mathematical convenience, we choose the Cartesian coordinate system in all the derivations. In addition, for notational simplicity, we employ the Einstein's summation convention in the mathematical expressions: if a certain index occurs twice in a term in the expression, the term is assumed to be summed over the repeated index for all admissible values of the index, e.g., $a_\alpha b_\alpha = \Sigma_{\alpha=1}^{3} a_\alpha b_\alpha$ in the three-dimensional coordinate systems. We first consider the two-body interaction modes (the bond-stretching and nonbonded LJ interactions), then the bond-bending (three-body interaction), and lastly the bond-torsional mode (four-body interaction).

1. Two-body interaction (the bond-stretching and nonbonded LJ interactions)

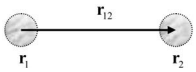

As in most cases, we assume that the two-body interaction depends only on the relative position vector between the two interacting atoms (say, 1 and 2), but independent of the center-of-mass position of the two atoms. Letting $\mathbf{r}_1$ ($\mathbf{F}_1$) and $\mathbf{r}_2$ ($\mathbf{F}_2$) the position (force) vectors of the first and the second atoms, respectively, and defining $\mathbf{r}_{12} \equiv \mathbf{r}_1 - \mathbf{r}_2$ and $r_{12} \equiv |\mathbf{r}_{12}|$, we can express $\nabla \cdot \mathbf{F}$ as

$$\nabla \cdot \mathbf{F} = \frac{\partial}{\partial \mathbf{r}_1} \cdot \mathbf{F}_1 + \frac{\partial}{\partial \mathbf{r}_2} \cdot \mathbf{F}_2 = \left(\frac{\partial}{\partial \mathbf{r}_1} - \frac{\partial}{\partial \mathbf{r}_2} \right) \cdot \mathbf{F}_1$$

$$= 2 \frac{\partial}{\partial \mathbf{r}_{12}} \cdot \mathbf{F}_1, \quad \text{(B1)}$$

where we used Newton's third law, $\mathbf{F}_2 = -\mathbf{F}_1$. Furthermore, in the case that the potential U (and thus force as well) is independent of the direction of $\mathbf{r}_{12}$ (i.e., central force fields, e.g., isotropic materials), we can write

$$\mathbf{F}_1 = -\frac{\partial U(r_{12})}{\partial \mathbf{r}_1} = -\frac{\partial U(r_{12})}{\partial \mathbf{r}_{12}} = -\frac{\partial U(r_{12})}{\partial r_{12}} \frac{\mathbf{r}_{12}}{r_{12}}. \quad \text{(B2)}$$

Putting Eq. (B2) in Eq. (B1), it is found to be

$$\nabla \cdot \mathbf{F} = -2 \left(\frac{d^2 U(r_{12})}{dr_{12}^2} + \frac{2}{r_{12}} \frac{dU(r_{12})}{dr_{12}} \right). \quad \text{(B3)}$$

2. The bond-bending interaction

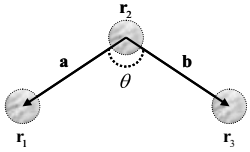

Assuming again the homogeneity of space (i.e., the bond-bending potential U_{ben} does not depend on the center-of-mass position $\mathbf{R}_G$), it is more convenient to transform the basis set of variables from the atomic position vectors $\{\mathbf{r}_1, \mathbf{r}_2, \mathbf{r}_3\}$ to the relative position and the center-of-mass vectors $\{\mathbf{a}, \mathbf{b}, \mathbf{R}_G\}$, where $\mathbf{a} = \mathbf{r}_1 - \mathbf{r}_2$, $\mathbf{b} = \mathbf{r}_3 - \mathbf{r}_2$, and $\mathbf{R}_G = (\mathbf{r}_1 + \mathbf{r}_2 + \mathbf{r}_3)/3$. Using the transformation rule, we can readily find the following relations between the two sets:

$$\left(\frac{\partial}{\partial \mathbf{r}_1} \right)_{\mathbf{r}_2, \mathbf{r}_3} = \left(\frac{\partial}{\partial \mathbf{a}} \right)_{\mathbf{b}, \mathbf{R}_G} + \frac{1}{3} \left(\frac{\partial}{\partial \mathbf{R}_G} \right)_{\mathbf{a}, \mathbf{b}}, \quad \text{(B4)}$$

$$\left(\frac{\partial}{\partial \mathbf{r}_2} \right)_{\mathbf{r}_1, \mathbf{r}_3} = -\left(\frac{\partial}{\partial \mathbf{a}} \right)_{\mathbf{b}, \mathbf{R}_G} - \left(\frac{\partial}{\partial \mathbf{b}} \right)_{\mathbf{a}, \mathbf{R}_G} + \frac{1}{3} \left(\frac{\partial}{\partial \mathbf{R}_G} \right)_{\mathbf{a}, \mathbf{b}}, \quad \text{(B5)}$$

$$\left(\frac{\partial}{\partial \mathbf{r}_3} \right)_{\mathbf{r}_1, \mathbf{r}_2} = \left(\frac{\partial}{\partial \mathbf{b}} \right)_{\mathbf{a}, \mathbf{R}_G} + \frac{1}{3} \left(\frac{\partial}{\partial \mathbf{R}_G} \right)_{\mathbf{a}, \mathbf{b}}. \quad \text{(B6)}$$

The force acting on each atom can be expressed based on the new variable set as

$$\mathbf{F}_1 = -\frac{\partial U_{\text{ben}}}{\partial \mathbf{r}_1} = -\frac{\partial U_{\text{ben}}}{\partial \mathbf{a}},$$

$$\mathbf{F}_2 = -\frac{\partial U_{\text{ben}}}{\partial \mathbf{r}_2} = \frac{\partial U_{\text{ben}}}{\partial \mathbf{a}} + \frac{\partial U_{\text{ben}}}{\partial \mathbf{b}}, \quad \text{(B7)}$$

$$\mathbf{F}_3 = -\frac{\partial U_{\text{ben}}}{\partial \mathbf{r}_3} = -\frac{\partial U_{\text{ben}}}{\partial \mathbf{b}},$$

since $\partial U_{\text{ben}} / \partial \mathbf{R}_G = 0$. Combining Eqs. (B4)–(B7), we can therefore express $\nabla \cdot \mathbf{F}$ as

$$\nabla \cdot \mathbf{F} = \frac{\partial}{\partial \mathbf{r}_1} \cdot \mathbf{F}_1 + \frac{\partial}{\partial \mathbf{r}_2} \cdot \mathbf{F}_2 + \frac{\partial}{\partial \mathbf{r}_3} \cdot \mathbf{F}_3$$
$$= \frac{\partial}{\partial \mathbf{a}} \cdot \mathbf{F}_1 - \frac{\partial}{\partial \mathbf{a}} \cdot \mathbf{F}_2 - \frac{\partial}{\partial \mathbf{b}} \cdot \mathbf{F}_2 + \frac{\partial}{\partial \mathbf{b}} \cdot \mathbf{F}_3$$
$$= -2\left(\frac{\partial}{\partial \mathbf{a}} \cdot \frac{\partial U_{\text{ben}}}{\partial \mathbf{a}} + \frac{\partial}{\partial \mathbf{a}} \cdot \frac{\partial U_{\text{ben}}}{\partial \mathbf{b}} + \frac{\partial}{\partial \mathbf{b}} \cdot \frac{\partial U_{\text{ben}}}{\partial \mathbf{b}} \right). \tag{B8}$$

In order to evaluate $\nabla \cdot \mathbf{F}$, we need to calculate the first and the second derivatives of $\cos\theta$ with respect to $\mathbf{a}$ and $\mathbf{b}$ from

$$\cos\theta = \frac{\mathbf{a} \cdot \mathbf{b}}{|\mathbf{a}||\mathbf{b}|}. \tag{B9}$$

The expressions for the first derivatives are derived as

$$\frac{\partial \cos\theta}{\partial a_\alpha} = \frac{b_\alpha}{|\mathbf{a}||\mathbf{b}|} - \frac{a_\alpha \cos\theta}{|\mathbf{a}|^2},$$
$$\frac{\partial \cos\theta}{\partial b_\alpha} = \frac{a_\alpha}{|\mathbf{a}||\mathbf{b}|} - \frac{b_\alpha \cos\theta}{|\mathbf{b}|^2}, \tag{B10}$$

where the subscript α represents the three Cartesian coordinates (x,y,z). From Eq. (B10), the expressions of the second derivatives are

$$\frac{\partial}{\partial a_\alpha}\frac{\partial \cos\theta}{\partial a_\alpha} = -\frac{2\cos\theta}{|\mathbf{a}|^2},$$
$$\frac{\partial}{\partial a_\alpha}\frac{\partial \cos\theta}{\partial b_\alpha} = \frac{1}{|\mathbf{a}||\mathbf{b}|}(1+\cos^2\theta), \tag{B11}$$
$$\frac{\partial}{\partial b_\alpha}\frac{\partial \cos\theta}{\partial b_\alpha} = -\frac{2\cos\theta}{|\mathbf{b}|^2}.$$

Furthermore, it is also apparent that

$$\left(\frac{\partial \cos\theta}{\partial a_\alpha}\right)\left(\frac{\partial \cos\theta}{\partial a_\alpha}\right) = \frac{\sin^2\theta}{|\mathbf{a}|^2},$$
$$\left(\frac{\partial \cos\theta}{\partial a_\alpha}\right)\left(\frac{\partial \cos\theta}{\partial b_\alpha}\right) = -\frac{\cos\theta \sin^2\theta}{|\mathbf{a}||\mathbf{b}|}, \tag{B12}$$
$$\left(\frac{\partial \cos\theta}{\partial b_\alpha}\right)\left(\frac{\partial \cos\theta}{\partial b_\alpha}\right) = \frac{\sin^2\theta}{|\mathbf{b}|^2}.$$

In addition, the following relations are valid:

$$\frac{\partial U_{\text{ben}}}{\partial \cos\theta} = -\frac{1}{\sin\theta}\frac{\partial U_{\text{ben}}}{\partial \theta},$$
$$\frac{\partial}{\partial \cos\theta}\left(\frac{\partial U_{\text{ben}}}{\partial \cos\theta}\right) = \frac{1}{\sin^2\theta}\left(\frac{\partial^2 U_{\text{ben}}}{\partial \theta^2} - \frac{\cos\theta}{\sin\theta}\frac{\partial U_{\text{ben}}}{\partial \theta}\right). \tag{B13}$$

Now, let us evaluate $\nabla \cdot \mathbf{F}$ of Eq. (B8). First, we express each term appearing on the right side of the last equality in Eq. (B8) as

$$\frac{\partial}{\partial \mathbf{a}} \cdot \frac{\partial U_{\text{ben}}}{\partial \mathbf{a}} = \frac{\partial}{\partial a_\alpha}\left(\frac{\partial U_{\text{ben}}}{\partial a_\alpha}\right)$$
$$= \frac{\partial}{\partial a_\alpha}\left(\frac{\partial U_{\text{ben}}}{\partial \cos\theta}\frac{\partial \cos\theta}{\partial a_\alpha}\right)$$
$$= \left(\frac{\partial \cos\theta}{\partial a_\alpha}\right)\frac{\partial}{\partial a_\alpha}\left(\frac{\partial U_{\text{ben}}}{\partial \cos\theta}\right) + \left(\frac{\partial U_{\text{ben}}}{\partial \cos\theta}\right)\frac{\partial}{\partial a_\alpha}\left(\frac{\partial \cos\theta}{\partial a_\alpha}\right)$$
$$= \left(\frac{\partial \cos\theta}{\partial a_\alpha}\right)\left(\frac{\partial \cos\theta}{\partial a_\alpha}\right)\frac{\partial}{\partial \cos\theta}\left(\frac{\partial U_{\text{ben}}}{\partial \cos\theta}\right) + \left(\frac{\partial U_{\text{ben}}}{\partial \cos\theta}\right)\frac{\partial}{\partial a_\alpha}\left(\frac{\partial \cos\theta}{\partial a_\alpha}\right), \tag{B14}$$

$$\frac{\partial}{\partial \mathbf{a}} \cdot \frac{\partial U_{\text{ben}}}{\partial \mathbf{b}} = \left(\frac{\partial \cos\theta}{\partial a_\alpha}\right)\left(\frac{\partial \cos\theta}{\partial b_\alpha}\right)\frac{\partial}{\partial \cos\theta}\left(\frac{\partial U_{\text{ben}}}{\partial \cos\theta}\right) + \left(\frac{\partial U_{\text{ben}}}{\partial \cos\theta}\right)\frac{\partial}{\partial a_\alpha}\left(\frac{\partial \cos\theta}{\partial b_\alpha}\right), \tag{B15}$$

$$\frac{\partial}{\partial \mathbf{b}} \cdot \frac{\partial U_{\text{ben}}}{\partial \mathbf{b}} = \left(\frac{\partial \cos\theta}{\partial b_\alpha}\right)\left(\frac{\partial \cos\theta}{\partial b_\alpha}\right)\frac{\partial}{\partial \cos\theta}\left(\frac{\partial U_{\text{ben}}}{\partial \cos\theta}\right) + \left(\frac{\partial U_{\text{ben}}}{\partial \cos\theta}\right)\frac{\partial}{\partial b_\alpha}\left(\frac{\partial \cos\theta}{\partial b_\alpha}\right). \tag{B16}$$

Inserting Eqs. (B14)–(B16) into Eq. (B8), we obtain

$$\nabla \cdot \mathbf{F} = -2\left(\frac{\partial}{\partial \mathbf{a}} \cdot \frac{\partial U_{\text{ben}}}{\partial \mathbf{a}} + \frac{\partial}{\partial \mathbf{a}} \cdot \frac{\partial U_{\text{ben}}}{\partial \mathbf{b}} + \frac{\partial}{\partial \mathbf{b}} \cdot \frac{\partial U_{\text{ben}}}{\partial \mathbf{b}} \right)$$
$$= -2\left\{ \frac{\partial}{\partial \cos\theta}\left(\frac{\partial U_{\text{ben}}}{\partial \cos\theta}\right)\left[\left(\frac{\partial \cos\theta}{\partial a_\alpha}\right)\left(\frac{\partial \cos\theta}{\partial a_\alpha}\right) + \left(\frac{\partial \cos\theta}{\partial a_\alpha}\right)\left(\frac{\partial \cos\theta}{\partial b_\alpha}\right) + \left(\frac{\partial \cos\theta}{\partial b_\alpha}\right)\left(\frac{\partial \cos\theta}{\partial b_\alpha}\right)\right] + \left(\frac{\partial U_{\text{ben}}}{\partial \cos\theta}\right)\left[\frac{\partial}{\partial a_\alpha}\left(\frac{\partial \cos\theta}{\partial a_\alpha}\right) + \frac{\partial}{\partial a_\alpha}\left(\frac{\partial \cos\theta}{\partial b_\alpha}\right) + \frac{\partial}{\partial b_\alpha}\left(\frac{\partial \cos\theta}{\partial b_\alpha}\right)\right]\right\}. \tag{B17}$$

Substituting Eqs. (B10)–(B13) into Eq. (B17), we finally arrive at the expression

$$\nabla \cdot \mathbf{F} = -2\left\{ \left(\frac{\partial^2 U_{\text{ben}}}{\partial \theta^2}\right)\left(\frac{1}{|\mathbf{a}|^2} + \frac{1}{|\mathbf{b}|^2} - \frac{\cos\theta}{|\mathbf{a}||\mathbf{b}|}\right) + \frac{\cos\theta}{\sin\theta}\frac{\partial U_{\text{ben}}}{\partial \theta}\left(\frac{1}{|\mathbf{a}|^2} + \frac{1}{|\mathbf{b}|^2} - \frac{1}{|\mathbf{a}||\mathbf{b}|\cos\theta}\right)\right\}. \tag{B18}$$

This equation can be applied to an arbitrary form of the bending potential as a function of θ. For example, $U_{\text{ben}}(\theta) = k_{\text{ben}}(\theta - \theta_{\text{eq}})^2/2$ as used in this study, Eq. (B18) gives rise to

$$\nabla \cdot \mathbf{F} = -2k_{\text{ben}}\left\{\left(\frac{1}{|\mathbf{a}|^2}+\frac{1}{|\mathbf{b}|^2}-\frac{\cos\theta}{|\mathbf{a}||\mathbf{b}|}\right)+\frac{\cos\theta}{\sin\theta}\left(\frac{1}{|\mathbf{a}|^2}+\frac{1}{|\mathbf{b}|^2}-\frac{1}{|\mathbf{a}||\mathbf{b}|\cos\theta}\right)(\theta-\theta_{\text{eq}})\right\}. \tag{B19}$$

3. The bond-torsional interaction

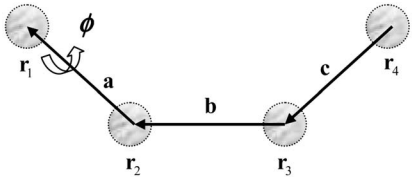

Let us again transform the variable set from the atomic position vectors $\{\mathbf{r}_1,\mathbf{r}_2,\mathbf{r}_3,\mathbf{r}_4\}$ to the relative position and the center-of-mass vectors, $\{\mathbf{a},\mathbf{b},\mathbf{c},\mathbf{R}_G\}$, where $\mathbf{a}=\mathbf{r}_1-\mathbf{r}_2$, $\mathbf{b}=\mathbf{r}_2-\mathbf{r}_3$, $\mathbf{c}=\mathbf{r}_3-\mathbf{r}_4$, and $\mathbf{R}_G=(\mathbf{r}_1+\mathbf{r}_2+\mathbf{r}_3+\mathbf{r}_4)/4$. We can then find the following transformation relations between the two sets:

$$\left(\frac{\partial}{\partial \mathbf{r}_1}\right)_{\mathbf{r}_2,\mathbf{r}_3,\mathbf{r}_4} = \left(\frac{\partial}{\partial \mathbf{a}}\right)_{\mathbf{b},\mathbf{c},\mathbf{R}_G} + \frac{1}{4}\left(\frac{\partial}{\partial \mathbf{R}_G}\right)_{\mathbf{a},\mathbf{b},\mathbf{c}}, \tag{B20}$$

$$\left(\frac{\partial}{\partial \mathbf{r}_2}\right)_{\mathbf{r}_1,\mathbf{r}_3,\mathbf{r}_4} = -\left(\frac{\partial}{\partial \mathbf{a}}\right)_{\mathbf{b},\mathbf{c},\mathbf{R}_G} + \left(\frac{\partial}{\partial \mathbf{b}}\right)_{\mathbf{a},\mathbf{c},\mathbf{R}_G} + \frac{1}{4}\left(\frac{\partial}{\partial \mathbf{R}_G}\right)_{\mathbf{a},\mathbf{b},\mathbf{c}}, \tag{B21}$$

$$\left(\frac{\partial}{\partial \mathbf{r}_3}\right)_{\mathbf{r}_1,\mathbf{r}_2,\mathbf{r}_4} = -\left(\frac{\partial}{\partial \mathbf{b}}\right)_{\mathbf{a},\mathbf{c},\mathbf{R}_G} + \left(\frac{\partial}{\partial \mathbf{c}}\right)_{\mathbf{a},\mathbf{b},\mathbf{R}_G} \frac{1}{4}\left(\frac{\partial}{\partial \mathbf{R}_G}\right)_{\mathbf{a},\mathbf{b},\mathbf{c}}, \tag{B22}$$

$$\left(\frac{\partial}{\partial \mathbf{r}_4}\right)_{\mathbf{r}_1,\mathbf{r}_2,\mathbf{r}_3} = -\left(\frac{\partial}{\partial \mathbf{c}}\right)_{\mathbf{a},\mathbf{b},\mathbf{R}_G} + \frac{1}{4}\left(\frac{\partial}{\partial \mathbf{R}_G}\right)_{\mathbf{a},\mathbf{b},\mathbf{c}}. \tag{B23}$$

Assuming again that the bond-torsional potential U_{tor} is independent of $\mathbf{R}_G$, we express the forces as

$$\mathbf{F}_1 = -\frac{\partial U_{\text{tor}}}{\partial \mathbf{a}}, \quad \mathbf{F}_2 = \frac{\partial U_{\text{tor}}}{\partial \mathbf{a}} - \frac{\partial U_{\text{tor}}}{\partial \mathbf{b}}, \quad \mathbf{F}_3 = \frac{\partial U_{\text{tor}}}{\partial \mathbf{b}} - \frac{\partial U_{\text{tor}}}{\partial \mathbf{c}}, \quad \mathbf{F}_4 = \frac{\partial U_{\text{tor}}}{\partial \mathbf{c}}. \tag{B24}$$

Combining Eqs. (B20)–(B24) and using a similar set of equations to Eqs. (B14)–(B16), $\nabla \cdot \mathbf{F}$ is found to be

$$\begin{aligned}\nabla \cdot \mathbf{F} &= \frac{\partial}{\partial \mathbf{r}_1}\cdot\mathbf{F}_1 + \frac{\partial}{\partial \mathbf{r}_2}\cdot\mathbf{F}_2 + \frac{\partial}{\partial \mathbf{r}_3}\cdot\mathbf{F}_3 + \frac{\partial}{\partial \mathbf{r}_4}\cdot\mathbf{F}_4 \\ &= -2\left(\frac{\partial}{\partial \mathbf{a}}\cdot\frac{\partial U_{\text{tor}}}{\partial \mathbf{a}} - \frac{\partial}{\partial \mathbf{a}}\cdot\frac{\partial U_{\text{tor}}}{\partial \mathbf{b}} + \frac{\partial}{\partial \mathbf{b}}\cdot\frac{\partial U_{\text{tor}}}{\partial \mathbf{b}} - \frac{\partial}{\partial \mathbf{b}}\cdot\frac{\partial U_{\text{tor}}}{\partial \mathbf{c}} + \frac{\partial}{\partial \mathbf{c}}\cdot\frac{\partial U_{\text{tor}}}{\partial \mathbf{c}}\right) \\ &= -2\frac{\partial}{\partial \cos\phi}\left(\frac{\partial U_{\text{tor}}}{\partial \cos\phi}\right)\left[\left(\frac{\partial \cos\phi}{\partial a_\alpha}\right)\left(\frac{\partial \cos\phi}{\partial a_\alpha}\right) + \left(\frac{\partial \cos\phi}{\partial b_\alpha}\right)\left(\frac{\partial \cos\phi}{\partial b_\alpha}\right) + \left(\frac{\partial \cos\phi}{\partial c_\alpha}\right)\left(\frac{\partial \cos\phi}{\partial c_\alpha}\right) - \left(\frac{\partial \cos\phi}{\partial a_\alpha}\right)\right. \\ &\quad \left.\times\left(\frac{\partial \cos\phi}{\partial b_\alpha}\right) - \left(\frac{\partial \cos\phi}{\partial b_\alpha}\right)\left(\frac{\partial \cos\phi}{\partial c_\alpha}\right)\right] - 2\left(\frac{\partial U_{\text{tor}}}{\partial \cos\phi}\right)\left[\frac{\partial}{\partial a_\alpha}\left(\frac{\partial \cos\phi}{\partial a_\alpha}\right) + \frac{\partial}{\partial b_\alpha}\left(\frac{\partial \cos\phi}{\partial b_\alpha}\right) + \frac{\partial}{\partial c_\alpha}\left(\frac{\partial \cos\phi}{\partial c_\alpha}\right)\right. \\ &\quad \left. - \frac{\partial}{\partial a_\alpha}\left(\frac{\partial \cos\phi}{\partial b_\alpha}\right) - \frac{\partial}{\partial b_\alpha}\left(\frac{\partial \cos\phi}{\partial c_\alpha}\right)\right].\end{aligned} \tag{B25}$$

Let us now evaluate the first and the second derivatives of $\cos\phi$ with respect to $\mathbf{a}$, $\mathbf{b}$, and $\mathbf{c}$. Here, we define $\cos\phi$ as

$$\cos\phi = \frac{(\mathbf{a}\times\mathbf{b})\cdot(\mathbf{b}\times\mathbf{c})}{|\mathbf{a}\times\mathbf{b}||\mathbf{b}\times\mathbf{c}|}, \tag{B26}$$

by taking $\phi=0$ as the *cis*-configuration. First, using the identity $(\mathbf{a}\times\mathbf{b})\cdot(\mathbf{b}\times\mathbf{c})=(\mathbf{a}\cdot\mathbf{b})(\mathbf{b}\cdot\mathbf{c})-(\mathbf{a}\cdot\mathbf{c})|\mathbf{b}|^2$, we derive

$$\frac{\partial}{\partial a_\alpha}[(\mathbf{a}\times\mathbf{b})\cdot(\mathbf{b}\times\mathbf{c})] = (\mathbf{b}\cdot\mathbf{c})b_\alpha - |\mathbf{b}|^2 c_\alpha, \tag{B27}$$

$$\frac{\partial}{\partial b_\alpha}[(\mathbf{a}\times\mathbf{b})\cdot(\mathbf{b}\times\mathbf{c})] = (\mathbf{b}\cdot\mathbf{c})a_\alpha + (\mathbf{a}\cdot\mathbf{b})c_\alpha - 2(\mathbf{a}\cdot\mathbf{c})b_\alpha, \tag{B28}$$

$$\frac{\partial}{\partial c_\alpha}[(\mathbf{a}\times\mathbf{b})\cdot(\mathbf{b}\times\mathbf{c})] = (\mathbf{a}\cdot\mathbf{b})b_\alpha - |\mathbf{b}|^2 a_\alpha, \tag{B29}$$

$$\frac{\partial}{\partial a_\alpha}[|\mathbf{a}\times\mathbf{b}||\mathbf{b}\times\mathbf{c}|] = \frac{|\mathbf{b}\times\mathbf{c}|}{|\mathbf{a}\times\mathbf{b}|}[|\mathbf{b}|^2 a_\alpha - (\mathbf{a}\cdot\mathbf{b})b_\alpha], \tag{B30}$$

$$\frac{\partial}{\partial b_\alpha}[|\mathbf{a}\times\mathbf{b}||\mathbf{b}\times\mathbf{c}|] = \frac{1}{|\mathbf{a}\times\mathbf{b}||\mathbf{b}\times\mathbf{c}|}\{|\mathbf{b}\times\mathbf{c}|^2[|\mathbf{a}|^2 b_\alpha - (\mathbf{a}\cdot\mathbf{b})a_\alpha] + |\mathbf{a}\times\mathbf{b}|^2[|\mathbf{c}|^2 b_\alpha - (\mathbf{b}\cdot\mathbf{c})c_\alpha]\}, \tag{B31}$$

$$\frac{\partial}{\partial c_\alpha}[|\mathbf{a}\times\mathbf{b}||\mathbf{b}\times\mathbf{c}|]=\frac{|\mathbf{a}\times\mathbf{b}|}{|\mathbf{b}\times\mathbf{c}|}[|\mathbf{b}|^2c_\alpha-(\mathbf{b}\cdot\mathbf{c})b_\alpha]. \tag{B32}$$

Then, from Eqs. (B26)–(B32), we obtain the following relations for the first derivatives:

$$\frac{\partial\cos\phi}{\partial a_\alpha}=\frac{(\mathbf{b}\cdot\mathbf{c})b_\alpha-|\mathbf{b}|^2c_\alpha}{|\mathbf{a}\times\mathbf{b}||\mathbf{b}\times\mathbf{c}|}+\cos\phi\left[\frac{(\mathbf{a}\cdot\mathbf{b})b_\alpha-|\mathbf{b}|^2a_\alpha}{|\mathbf{a}\times\mathbf{b}|^2}\right], \tag{B33}$$

$$\frac{\partial\cos\phi}{\partial b_\alpha}=\frac{(\mathbf{b}\cdot\mathbf{c})a_\alpha+(\mathbf{a}\cdot\mathbf{b})c_\alpha-2(\mathbf{a}\cdot\mathbf{c})b_\alpha}{|\mathbf{a}\times\mathbf{b}||\mathbf{b}\times\mathbf{c}|}+\cos\phi\left[\frac{(\mathbf{a}\cdot\mathbf{b})a_\alpha-|\mathbf{a}|^2b_\alpha}{|\mathbf{a}\times\mathbf{b}|^2}+\frac{(\mathbf{b}\cdot\mathbf{c})c_\alpha-|\mathbf{c}|^2b_\alpha}{|\mathbf{b}\times\mathbf{c}|^2}\right], \tag{B34}$$

$$\frac{\partial\cos\phi}{\partial c_\alpha}=\frac{(\mathbf{a}\cdot\mathbf{b})b_\alpha-|\mathbf{b}|^2a_\alpha}{|\mathbf{a}\times\mathbf{b}||\mathbf{b}\times\mathbf{c}|}+\cos\phi\left[\frac{(\mathbf{b}\cdot\mathbf{c})b_\alpha-|\mathbf{b}|^2c_\alpha}{|\mathbf{b}\times\mathbf{c}|^2}\right]. \tag{B35}$$

Furthermore, the second derivatives are found to be

$$\frac{\partial}{\partial a_\alpha}\frac{\partial\cos\phi}{\partial a_\alpha}=-\frac{|\mathbf{b}|^2}{|\mathbf{a}\times\mathbf{b}|^2}\cos\phi, \tag{B36}$$

$$\begin{aligned}\frac{\partial}{\partial b_\alpha}\frac{\partial\cos\phi}{\partial b_\alpha}=&2\frac{1}{|\mathbf{a}\times\mathbf{b}||\mathbf{b}\times\mathbf{c}|}\left\{\frac{(\mathbf{a}\cdot\mathbf{b})[(\mathbf{a}\cdot\mathbf{b})(\mathbf{a}\cdot\mathbf{c})-|\mathbf{a}|^2(\mathbf{b}\cdot\mathbf{c})]}{|\mathbf{a}\times\mathbf{b}|^2}+\frac{(\mathbf{b}\cdot\mathbf{c})[(\mathbf{a}\cdot\mathbf{c})(\mathbf{b}\cdot\mathbf{c})-|\mathbf{c}|^2(\mathbf{a}\cdot\mathbf{b})]}{|\mathbf{b}\times\mathbf{c}|^2}+2(\mathbf{a}\cdot\mathbf{c})\right\}\\&+\cos\phi\left\{\frac{2|\mathbf{a}|^2}{|\mathbf{a}\times\mathbf{b}|^2}+\frac{2|\mathbf{c}|^2}{|\mathbf{b}\times\mathbf{c}|^2}+\frac{(\mathbf{b}\cdot\mathbf{c})[(\mathbf{a}\cdot\mathbf{b})(\mathbf{a}\cdot\mathbf{c})-|\mathbf{a}|^2(\mathbf{b}\cdot\mathbf{c})]}{|\mathbf{a}\times\mathbf{b}|^2|\mathbf{b}\times\mathbf{c}|^2}+\frac{(\mathbf{a}\cdot\mathbf{b})[(\mathbf{a}\cdot\mathbf{c})(\mathbf{b}\cdot\mathbf{c})-|\mathbf{c}|^2(\mathbf{a}\cdot\mathbf{b})]}{|\mathbf{a}\times\mathbf{b}|^2|\mathbf{b}\times\mathbf{c}|^2}\right\},\end{aligned} \tag{B37}$$

$$\frac{\partial}{\partial c_\alpha}\frac{\partial\cos\phi}{\partial c_\alpha}=-\frac{|\mathbf{b}|^2}{|\mathbf{b}\times\mathbf{c}|^2}\cos\phi, \tag{B38}$$

$$\frac{\partial}{\partial a_\alpha}\frac{\partial\cos\phi}{\partial b_\alpha}=\frac{(\mathbf{b}\cdot\mathbf{c})}{|\mathbf{a}\times\mathbf{b}||\mathbf{b}\times\mathbf{c}|}(1+\sin^2\phi)+\frac{(\mathbf{a}\cdot\mathbf{b})}{|\mathbf{a}\times\mathbf{b}|^2}\cos\phi, \tag{B39}$$

$$\frac{\partial}{\partial b_\alpha}\frac{\partial\cos\phi}{\partial c_\alpha}=\frac{(\mathbf{a}\cdot\mathbf{b})}{|\mathbf{a}\times\mathbf{b}||\mathbf{b}\times\mathbf{c}|}(1+\sin^2\phi)+\frac{(\mathbf{b}\cdot\mathbf{c})}{|\mathbf{b}\times\mathbf{c}|^2}\cos\phi. \tag{B40}$$

The second-order terms with respect to the first derivatives are also found to be

$$\left(\frac{\partial\cos\phi}{\partial a_\alpha}\right)\left(\frac{\partial\cos\phi}{\partial a_\alpha}\right)=\frac{|\mathbf{b}|^2}{|\mathbf{a}\times\mathbf{b}|^2}\sin^2\phi, \tag{B41}$$

$$\begin{aligned}\left(\frac{\partial\cos\phi}{\partial b_\alpha}\right)\left(\frac{\partial\cos\phi}{\partial b_\alpha}\right)=&-\frac{1}{|\mathbf{a}\times\mathbf{b}|^2|\mathbf{b}\times\mathbf{c}|^2}\{(\mathbf{b}\cdot\mathbf{c})[(\mathbf{a}\cdot\mathbf{b})(\mathbf{a}\cdot\mathbf{c})-|\mathbf{a}|^2(\mathbf{b}\cdot\mathbf{c})]+(\mathbf{a}\cdot\mathbf{b})[(\mathbf{a}\cdot\mathbf{c})(\mathbf{b}\cdot\mathbf{c})-|\mathbf{c}|^2(\mathbf{a}\cdot\mathbf{b})]\}\\&+2\cos\phi\left\{\frac{(\mathbf{a}\cdot\mathbf{b})[(\mathbf{a}\cdot\mathbf{b})(\mathbf{a}\cdot\mathbf{c})-|\mathbf{a}|^2(\mathbf{b}\cdot\mathbf{c})]}{|\mathbf{a}\times\mathbf{b}|^3|\mathbf{b}\times\mathbf{c}|}+\frac{2(\mathbf{a}\cdot\mathbf{c})}{|\mathbf{a}\times\mathbf{b}||\mathbf{b}\times\mathbf{c}|}+\frac{(\mathbf{b}\cdot\mathbf{c})[(\mathbf{a}\cdot\mathbf{c})(\mathbf{b}\cdot\mathbf{c})-|\mathbf{c}|^2(\mathbf{a}\cdot\mathbf{b})]}{|\mathbf{a}\times\mathbf{b}||\mathbf{b}\times\mathbf{c}|^3}\right\}\\&+\cos^2\phi\left\{\frac{3|\mathbf{a}|^2}{|\mathbf{a}\times\mathbf{b}|^2}+\frac{|\mathbf{c}|^2}{|\mathbf{b}\times\mathbf{c}|^2}+\frac{2(\mathbf{a}\cdot\mathbf{b})[(\mathbf{a}\cdot\mathbf{c})(\mathbf{b}\cdot\mathbf{c})-|\mathbf{c}|^2(\mathbf{a}\cdot\mathbf{b})]}{|\mathbf{a}\times\mathbf{b}|^2|\mathbf{b}\times\mathbf{c}|^2}\right\},\end{aligned} \tag{B42}$$

$$\left(\frac{\partial\cos\phi}{\partial c_\alpha}\right)\left(\frac{\partial\cos\phi}{\partial c_\alpha}\right)=\frac{|\mathbf{b}|^2}{|\mathbf{b}\times\mathbf{c}|^2}\sin^2\phi, \tag{B43}$$

$$\left(\frac{\partial\cos\phi}{\partial a_\alpha}\right)\left(\frac{\partial\cos\phi}{\partial b_\alpha}\right)=-\frac{(\mathbf{a}\cdot\mathbf{b})}{|\mathbf{a}\times\mathbf{b}|^2}\sin^2\phi-\frac{(\mathbf{b}\cdot\mathbf{c})}{|\mathbf{a}\times\mathbf{b}||\mathbf{b}\times\mathbf{c}|}\cos\phi\sin^2\phi, \tag{B44}$$

$$\left(\frac{\partial\cos\phi}{\partial b_\alpha}\right)\left(\frac{\partial\cos\phi}{\partial c_\alpha}\right)=-\frac{(\mathbf{b}\cdot\mathbf{c})}{|\mathbf{b}\times\mathbf{c}|^2}\sin^2\phi-\frac{(\mathbf{a}\cdot\mathbf{b})}{|\mathbf{a}\times\mathbf{b}||\mathbf{b}\times\mathbf{c}|}\cos\phi\sin^2\phi. \tag{B45}$$

Using all of these derivatives, Eqs. (B33)–(B45), together with a simple evaluation of the first and the second derivatives of $U_{\mathrm{tor}}(\phi)$ with respect to $\cos\phi$, we evaluate $\nabla\cdot\mathbf{F}$ in Eq. (B25).

[1] L. D. Landau and E. M. Lifshitz, *Course of Theoretical Physics*, 3rd ed. (Butterworth-Heinemann, Oxford, 1976), Vol. 5.
[2] R. C. Tolman, *The Principles of Statistical Mechanics* (Oxford University Press, London, 1938).
[3] H. H. Rugh, Phys. Rev. Lett. **78**, 772 (1997); J. Phys. A **31**, 7761 (1998).
[4] B. D. Butler, G. Ayton, O. G. Jepps, and D. J. Evans, J. Chem. Phys. **109**, 6519 (1998).
[5] G. Ayton, O. G. Jepps, and D. J. Evans, Mol. Phys. **96**, 915 (1999).
[6] O. G. Jepps, G. Ayton, and D. J. Evans, Phys. Rev. E **62**, 4757 (2000).
[7] L. Lue, O. G. Jepps, J. Delhommelle, and D. J. Evans, Mol. Phys. **100**, 2387 (2002).
[8] J. Delhommelle and D. J. Evans, J. Chem. Phys. **114**, 6229 (2001); **114**, 6236 (2001).
[9] Y. Han and D. G. Grier, Phys. Rev. Lett. **92**, 148301 (2004).
[10] P. Pliego-Pastrana and M. D. Carbajal-Tinoco, J. Chem. Phys. **122**, 244908 (2005).
[11] R. S. Saksena and L. V. Woodcock, J. Chem. Phys. **122**, 164501 (2005).
[12] G. Rickayzen and D. M. Heyes, J. Chem. Phys. **127**, 144512 (2007).
[13] C. Braga and K. P. Travis, J. Chem. Phys. **123**, 134101 (2005).
[14] J. Delhommelle and D. J. Evans, J. Chem. Phys. **115**, 43 (2001).
[15] J. Delhommelle and D. J. Evans, J. Chem. Phys. **117**, 6016 (2002).
[16] C. Baig, B. J. Edwards, D. J. Keffer, and H. D. Cochran, J. Chem. Phys. **122**, 114103 (2005); B. J. Edwards, C. Baig, and D. J. Keffer, *ibid.* **123**, 114106 (2005).
[17] C. Baig and V. G. Mavrantzas, Phys. Rev. Lett. **99**, 257801 (2007); Phys. Rev. B **79**, 144302 (2009).
[18] D. Jou, J. Casas-Vázquez, and G. Lebon, Rep. Prog. Phys. **51**, 1105 (1988).
[19] J. Casas-Vázquez and D. Jou, Phys. Rev. E **49**, 1040 (1994).
[20] S. R. de Groot and P. Mazur, *Non-equilibrium Thermodynamics* (North-Holland, Amsterdam, 1962).
[21] R. J. J. Jongschaap, Rep. Prog. Phys. **53**, 1 (1990); J. Non-Newtonian Fluid Mech. **96**, 63 (2001).
[22] A. N. Beris and B. J. Edwards, *Thermodynamics of Flowing Systems* (Oxford University Press, New York, 1994).
[23] H. C. Öttinger, *Beyond Equilibrium Thermodynamics* (Wiley-Interscience, New Jersey, 2004).
[24] C. Baig, B. J. Edwards, D. J. Keffer, H. D. Cochran, and V. A. Harmandaris, J. Chem. Phys. **124**, 084902 (2006).
[25] S. Nosé, Mol. Phys. **52**, 255 (1984); W. G. Hoover, Phys. Rev. A **31**, 1695 (1985).
[26] C. Baig, B. J. Edwards, D. J. Keffer, and H. D. Cochran, J. Chem. Phys. **122**, 184906 (2005).
[27] M. Tuckerman, B. J. Berne, and G. J. Martyna, J. Chem. Phys. **97**, 1990 (1992).
[28] A. W. Lees and S. F. Edwards, J. Phys. C **5**, 1921 (1972).
[29] A. M. Kraynik and D. A. Reinelt, Int. J. Multiphase Flow **18**, 1045 (1992).
[30] B. D. Todd and P. J. Daivis, Phys. Rev. Lett. **81**, 1118 (1998); Comput. Phys. Commun. **117**, 191 (1999).
[31] V. G. Mavrantzas and H. C. Öttinger, Macromolecules **35**, 960 (2002).
[32] R. B. Bird, C. F. Curtiss, R. C. Armstrong, and O. Hassager, *Dynamics of Polymeric Liquids, Kinetic Theory*, 2nd ed. (Wiley, New York, 1987), Vol. 2.
[33] V. G. Mavrantzas and D. N. Theodorou, Macromolecules **31**, 6310 (1998).
[34] H. B. Callen, *Thermodynamics and an Introduction to Thermostatistics*, 2nd ed. (Wiley, New York, 1985).
[35] P. V. K. Pant and D. N. Theodorou, Macromolecules **28**, 7224 (1995); V. G. Mavrantzas, T. D. Boone, E. Zervopoulou, and D. N. Theodorou, *ibid.* **32**, 5072 (1999).
[36] J. I. Siepmann, S. Karaborni, and B. Smit, Nature (London) **365**, 330 (1993).
[37] J. D. Weeks, D. Chandler, and H. C. Andersen, J. Chem. Phys. **54**, 5237 (1971).
[38] M. P. Allen and D. J. Tildesley, *Computer Simulation of Liquids* (Clarendon, Oxford, 1987).
[39] J. M. Kim, B. J. Edwards, D. J. Keffer, and B. Khomami, Phys. Lett. A **373**, 769 (2009).
[40] T. C. Ionescu, B. J. Edwards, and V. G. Mavrantzas, J. Rheol. **52**, 105 (2008).
[41] T. C. Ionescu, V. G. Mavrantzas, and B. J. Edwards, J. Rheol. **52**, 567 (2008).
[42] U. Gaur and B. Wunderlich, J. Phys. Chem. Ref. Data **10**, 119 (1981).
[43] C. Baig and B. J. Edwards, Europhys. Lett. **89**, 36003 (2010).
[44] C. Baig and B. J. Edwards, "Atomistic simulation of crystallization of a polyethylene melt in steady uniaxial extension," J. Non-Newtonian Fluid Mech. (to be published).
[45] P. Ilg (personal communication).